

2

NAVAL POSTGRADUATE SCHOOL Monterey, California



AD-A219 645

THESIS

SEP 1989
D

FLOWFIELD MEASUREMENTS
IN THE WAKE OF A MISSILE
AT HIGH ANGLE OF ATTACK

by

Dan A. Johnson

September 1989

Thesis Advisor:

Richard M. Howard

Approved for public release: distribution is unlimited.

90 08 23 036

REPORT DOCUMENTATION PAGE				Form Approved OMB No 0704-0188	
1a REPORT SECURITY CLASSIFICATION Unclassified			1b RESTRICTIVE MARKINGS		
2a SECURITY CLASSIFICATION AUTHORITY			3 DISTRIBUTION/AVAILABILITY OF REPORT Approved for public release; distribution is unlimited		
2b DECLASSIFICATION/DOWNGRADING SCHEDULE					
4 PERFORMING ORGANIZATION REPORT NUMBER(S)			5 MONITORING ORGANIZATION REPORT NUMBER(S)		
6a NAME OF PERFORMING ORGANIZATION Naval Postgraduate School		6b OFFICE SYMBOL (If applicable) 67	7a NAME OF MONITORING ORGANIZATION Naval Postgraduate School		
6c ADDRESS (City, State, and ZIP Code) Monterey, CA 93943			7b ADDRESS (City, State, and ZIP Code) Monterey, CA 93943		
8a NAME OF FUNDING / SPONSORING ORGANIZATION		8b OFFICE SYMBOL (If applicable)	9 PROCUREMENT INSTRUMENT IDENTIFICATION NUMBER		
8c ADDRESS (City, State, and ZIP Code)			10 SOURCE OF FUNDING NUMBERS		
			PROGRAM ELEMENT NO	PROJECT NO	TASK NO
					WORK UNIT ACCESSION NO
11 TITLE (Include Security Classification) FLOWFIELD MEASUREMENTS IN THE WAKE OF A MISSILE AT HIGH ANGLE OF ATTACK					
12 PERSONAL AUTHOR(S) Johnson, Dan A.					
13a TYPE OF REPORT Master's Thesis		13b TIME COVERED FROM _____ TO _____		14 DATE OF REPORT (Year, Month, Day) 1989 September	
15 PAGE COUNT 74					
16 SUPPLEMENTARY NOTATION The views expressed in this thesis are those of the author and do not reflect the official policy of the Department of Defense or the U.S. Government.					
17 COSATI CODES			18 SUBJECT TERMS (Continue on reverse if necessary and identify by block number)		
FIELD	GROUP	SUB-GROUP	Vertical Launch; Surface-to-Air Missile; High Angle of Attack Aerodynamics; Turbulence; Body of Revolution; Vortex Asymmetry. (hd)		
19 ABSTRACT (Continue on reverse if necessary and identify by block number) 110,000 The flowfield about a vertically-launched surface-to-air missile model at an angle of attack of 50 degrees and a Reynolds number of 1.1×10^6 was investigated in a low-speed wind tunnel at the Naval Postgraduate School. Determined were the location and intensity of the asymmetric vortices in the wake of the model using planar velocity vector, total pressure coefficient, and vorticity plots. Two model configurations were tested: one at a roll angle of 0 degrees (the '+' configuration) and the other at a roll angle of 45 degrees (the 'x' configuration). Two flowfield conditions were used: one with no turbulence and the other with turbulence of a length scale on the order of the size of the nose-generated vortices. The following conclusions were reached: 1) the addition of turbulence changed the magnitudes of the variables without changing the patterns in the plots; 2) changing roll angle significantly altered the patterns of the plots; 3) in general, the locations of the vortices as indicated by the velocity plots do not coincide with the centers for the pressure or vorticity plots; 4) total pressure losses coincide with changes in magnitude of side force as noted in an earlier study. <i>Key words: Thesis.</i>					
20 DISTRIBUTION/AVAILABILITY OF ABSTRACT <input checked="" type="checkbox"/> UNCLASSIFIED/UNLIMITED <input type="checkbox"/> SAME AS RPT <input type="checkbox"/> DTIC USERS			21 ABSTRACT SECURITY CLASSIFICATION Unclassified		
22a NAME OF RESPONSIBLE INDIVIDUAL Richard M. Howard			22b TELEPHONE (Include Area Code) (408) 646-2870		22c OFFICE SYMBOL Code 67Ho

Approved for public release; distribution is unlimited.

Flowfield Measurements
in the Wake of a Missile
at High Angle of Attack

by

Dan A. Johnson
Captain, United States Army
B.S., United States Military Academy, 1979

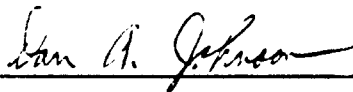
Submitted in partial fulfillment
of the requirements for the degree of

MASTER OF SCIENCE IN AERONAUTICAL ENGINEERING

from the

NAVAL POSTGRADUATE SCHOOL
September 1989

Author:

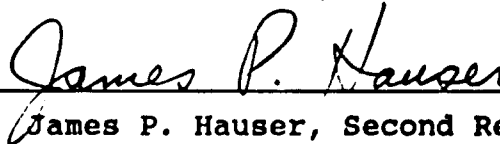


Dan A. Johnson

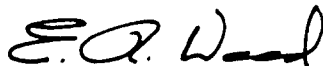
Approved by:



Richard M. Howard, Thesis Advisor



James P. Hauser, Second Reader



E. Roberts Wood, Chairman
Department of Aeronautics and Astronautics

ABSTRACT

The flowfield about a vertically-launched surface-to-air missile model at an angle of attack of 50 degrees and a Reynolds number of 1.1×10^5 was investigated in a low-speed wind tunnel at the Naval Postgraduate School. Determined were the location and intensity of the asymmetric vortices in the wake of the model using planar velocity vector, total pressure coefficient, and vorticity plots. Two model configurations were tested: one at a roll angle of 0 degrees (the "+" configuration) and the other at a roll angle of 45 degrees (the "x" configuration). Two flowfield conditions were used: one with no turbulence and the other with turbulence of a length scale on the order of the size of the nose-generated vortices. The following conclusions were reached: 1) the addition of turbulence changed the magnitudes of the variables without changing the patterns in the plots; 2) changing roll angle significantly altered the patterns of the plots; 3) in general, the locations of the vortices as indicated by the velocity plots do not coincide with the centers for the pressure or vorticity plots; 4) total pressure losses coincide with changes in magnitude of side force as noted in an earlier study.

iii



Accession For	
NTIS GASI	<input checked="" type="checkbox"/>
DTIC TAB	<input type="checkbox"/>
Unannounced	<input type="checkbox"/>
Justification	
By	
Distribution/	
Availability Codes	
Avail and/or	
Dist	Special
A-1	

THESIS DISCLAIMER

The reader is cautioned that computer programs developed in this research may not have been exercised for all cases of interest. While every effort has been made, within the time available, to ensure that the programs are free of computational and logic errors, they cannot be considered validated. Any application of these programs without additional verification is at the risk of the user.

TABLE OF CONTENTS

I.	INTRODUCTION	1
	A. HIGH ANGLE OF ATTACK AERODYNAMICS	2
	B. TURBULENCE	4
	C. PURPOSE	5
II.	EXPERIMENT AND PROCEDURE	8
	A. OVERVIEW	8
	B. EQUIPMENT	8
	C. SURVEY GRID	13
	D. TEST CONDITIONS	16
	E. EXPERIMENTAL VARIABLES	17
	F. PROCEDURE	19
III.	RESULTS	21
	A. INTRODUCTION	21
	B. CONFIGURATION 0A	22
	C. CONFIGURATION 3A	28
	D. CONFIGURATION 0C	34
	E. CONFIGURATION 3C	40
	F. COMPARISON BETWEEN NO TURBULENCE AND TURBULENCE	46
	G. COMPARISON BETWEEN ROLL ANGLES	46

IV. CONCLUSIONS AND RECOMMENDATIONS	40
APPENDIX A	56
APPENDIX B	56
APPENDIX C	56
LIST OF REFERENCES	60
INITIAL DISTRIBUTION LIST	60

LIST OF FIGURES

Figure

1.	Flow Regimes	3
2.	NPS Low-speed Wind Tunnel.	9
3.	Missile Model Dimensions	10
4.	Mounting Arm Assembly.	11
5.	Survey Grid Location	14
6.	Survey Grid Dimensions	15
7.	Velocity Vectors - Configuration 0A.	24
8.	Total Pressure Coefficient - Configuration 0A.	25
9.	Vorticity - Configuration 0A	26
10.	Vorticity (at 6d) - Configuration 0A	27
11.	Velocity Vectors - Configuration 3A.	30
12.	Total Pressure Coefficient - Configuration 3A.	31
13.	Vorticity - Configuration 3A	32
14.	Vorticity (at 6d) - Configuration 3A	33
15.	Velocity Vectors - Configuration 0C.	36
16.	Total Pressure Coefficient - Configuration 0C.	37
17.	Vorticity - Configuration 0C	38
18.	Vorticity (at 6d) - Configuration 0C	39
19.	Velocity Vectors - Configuration 3C.	42

20.	Total Pressure Coefficient - Configuration 3C. . . .	43
21.	Vorticity - Configuration 3C	44
22.	Vorticity (at 6d) - Configuration 3C	45

ACKNOWLEDGEMENTS

My sincere gratitude goes to my thesis advisor, Dr. Richard Howard, for his guidance and assistance in my study of high angle of attack aerodynamics.

I would also like to thank the following Naval Postgraduate School personnel for their assistance:

Mr. Jack King, Aerolab

Lt. J.J. Viniotis, USN, NPS Student

Lt. Jim Pinaire, USN, NPS Student

I. INTRODUCTION

In high angle of attack aerodynamics flow separation, in the form of asymmetric vortices, influences the side and normal forces generated on a missile. Major factors that influence separation are nose shape, angle of attack, crossflow Reynolds number, and nose fineness ratio. Other factors include roll angle and rate, freestream turbulence, surface roughness, acoustic vibrations, and missile vibrations. [Ref. 1, 2, 3]

An example of a missile that could experience the side force variations is the vertically-launched surface-to-air missile (VLSAM). At launch, it could encounter large crosswinds and turbulence caused by interaction of the wind with the ocean's surface and the superstructure of the ship. This environment, when combined with the missile's relatively slow initial velocity, causes the missile to be in a high angle of attack regime, which may result in the formation of asymmetric vortices along the length of the missile. These vortices affect the side forces on the missile and can affect its controllability. A vertically-launched anti-submarine rocket was lost due to asymmetric vortices caused by its high angle of attack and nose asymmetry [Ref 4].

A. HIGH ANGLE OF ATTACK AERODYNAMICS

As a slender body of revolution increases in angle of attack from 0 to 90 degrees, it encounters four distinct flow regimes [Ref. 5]. Figure 1 shows sketches of the four regimes. At angles of attack less than 5 degrees, axial flow dominates and there is no discernable separation. Between 5 and 20 degrees, separation occurs on the lee side and a pair of symmetric vortices is formed. There are no side or yawing forces produced. Between 20 and 60 degrees, vortices may form asymmetrically. This asymmetry generates side and yawing forces with greater asymmetry generating the largest side force magnitude [Ref. 6]. Between 60 and 90 degrees, the separation becomes unsteady. Reynolds number, Mach number, and geometry determine whether the boundary layer separates as a von Karman vortex sheet or a wake-like flow [Refs. 7, 8].

For angles of attack between 20 and 60 degrees, nose-generated asymmetric vortices may appear in the flowfield around an ogive-nosed, slender, cylindrical body. These occur along the entire body length and induce significant side forces on the body [Ref. 8]. They also tend to dominate the vortices formed by afterbody geometry, although the positioning and strength of the afterbody vortices can be influenced by the afterbody geometry. The addition of wings to a body moves the nose vortices closer to the body [Refs. 7, 9, 10]. Some researchers have found that strakes reduce

the effects of vortices. Rabang has shown that the addition of wings and strakes, depending on the configuration, maintained the effects of the vortices [Ref. 10].

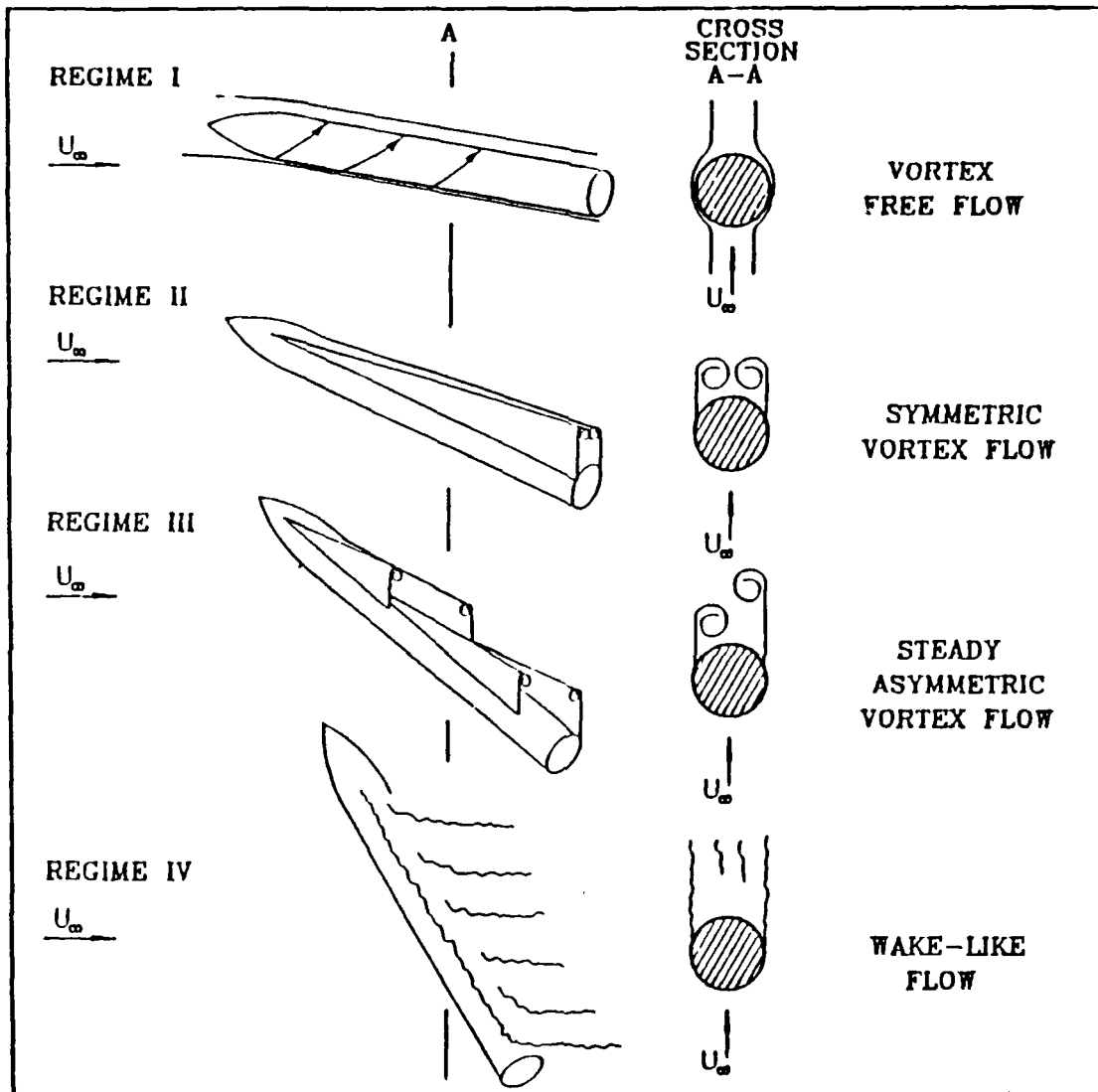


Figure 1. Flow Regimes [Ref. 5]

B. TURBULENCE

Turbulence denotes the presence of random, short duration variations in a flow field with a given mean velocity. When calculating turbulence effects on a body, a comparison between the scale of the body and the turbulence must be made. Turbulence intensity is the measure of the relative magnitude of velocity fluctuations in the flowfield. Higher intensities indicate higher kinetic energy and more turbulent flow. [Ref. 10]

Turbulence length scales are a special measure of the fluid disturbance eddies. An increase in the turbulence length corresponds to an increase in time the body is exposed to the fluctuations. Length-scale-to-body-size ratio may determine the manner in which turbulence affects the missile flowfield [Refs. 10, 11]. If the length scale is much greater than the body, the effect on the missile is essentially the same as a steady-state flowfield. If the length scale is on the order of that of the body, large effects on the body can be noted [Ref. 12]. If the length scale is much smaller, especially smaller than the diameter, the turbulence affects the boundary layer development and separation [Ref. 13].

Boundary-layer-scale turbulence adds energy to the boundary layer which delays separation of the turbulent boundary layer. This delay reduces the asymmetry of the

separation and thus reduces the asymmetric-vortex-induced side forces. [Refs. 13, 14]

Turbulence with a length scale on the order of vortices created by the missile body can influence the position of the asymmetric vortices and subsequently, the side forces on the body. Kabang noted that turbulence intensity with a length scale on the order of the nose-generated vortices tended to increase or maintain the side force compared to other length scales which reduced the side force.

In the ocean environment, the turbulence length scales are much larger than the missile diameter. This would indicate very little influence on the missile as discussed previously. However, the length scale of the turbulence is decreased by a cascade effect. This effect occurs as disturbances in the flowfield experience strain. The strain causes large-length-scale turbulence to become smaller. The smaller-length-scale turbulence may be on the order of the missile diameter or smaller. It then begins to influence the boundary layer and separation behavior. How much of the turbulent energy is of a scale small enough to make the high intensity level effective remains unknown. [Ref. 10]

C. PURPOSE

This thesis is part of an on-going research effort into the effects of vortex-length-scale turbulence and missile

geometry on the aerodynamic characteristics of the missile. Rabang [Ref. 10] studied the effects of turbulence in the flowfield and wing geometry on the aerodynamic forces of the missile. He concluded that turbulence with length scales on the order of the nose-generated vortices tended to increase the side-force magnitude and to decrease the flow unsteadiness. Further increasing the length scales tended to reduce the magnitude of the side force. He verified that nose roll angle can cause significant changes in the side forces. He also found that the addition of low-aspect-ratio wings did not significantly change the magnitude of the side force.

Lung [Ref. 7] used pressure measurements in the flowfield to locate and measure characteristics of the vortices in the flow around a missile without wings in turbulent and non-turbulent flow. He concluded that the strength of the vortices, as measured by total pressure losses, decreased and the vortices became more diffuse with the addition of turbulence.

Viniotis [Ref. 8] used pressure measurements in the flow field to locate and measure characteristics of vortices in the flow around a missile with two wing configurations in turbulent and non-turbulent flow. He concluded that the addition of turbulence tended to decrease the strength and intensity of the vortices. He also concluded that the addition of wings/strakes caused the vortices to move closer

to the missile body, as previously noted by earlier investigators.

The purpose of this research was to locate and measure the characteristics of the vortices for two wing configurations in turbulent and non-turbulent flow at a position $11d$ (11 missile diameters, versus $6d$ used by Viniotis and Lung) from the nose of the missile. By comparing the results with Viniotis and Rabang, correlations between the vortices at $6d$ and $11d$ from the missile nose and the aerodynamic forces will be made.

II. EXPERIMENT AND PROCEDURE

A. OVERVIEW

Pressure measurements were made in the wake of a missile model at high angle of attack to study the behavior of the asymmetric vortices. Four experimental conditions were used. The missile was positioned at two different roll angles, and freestream conditions were with and without turbulence of a scale of the order of the nose-generated vortices. Pressure measurements were converted to total and planar velocity components, total and static pressure coefficients, and vorticity. These variables were plotted to determine the characteristics of the vortices.

B. EQUIPMENT

The major pieces of experimental equipment were the NPS wind tunnel, the VLSAM model, the three-axis traverser, the five-hole pressure probe, the data acquisition system, and the data reduction/display software.

The low-speed wind tunnel at the Naval Postgraduate School is a low-speed, single-return, horizontal-flow tunnel powered by a 100-horsepower electric motor with a three-bladed variable-pitch fan. It has a contraction ratio of approximately 10:1 and the test section measures 45 inches by

28 inches. The tunnel was designed to provide velocities up to 290 feet per second (Figure 2, [Ref. 15]).

Figure 3 depicts the specifications of the missile model. It is made of aluminum alloy and has detachable wings/strakes and tails and can be mounted at various roll angles in 45 degree increments [Ref. 10]. It was mounted with a sting mount attached to a rotating arm that pivoted at the top and bottom of the tunnel (Figure 4), allowing angle of attack to be varied in a horizontal plane.

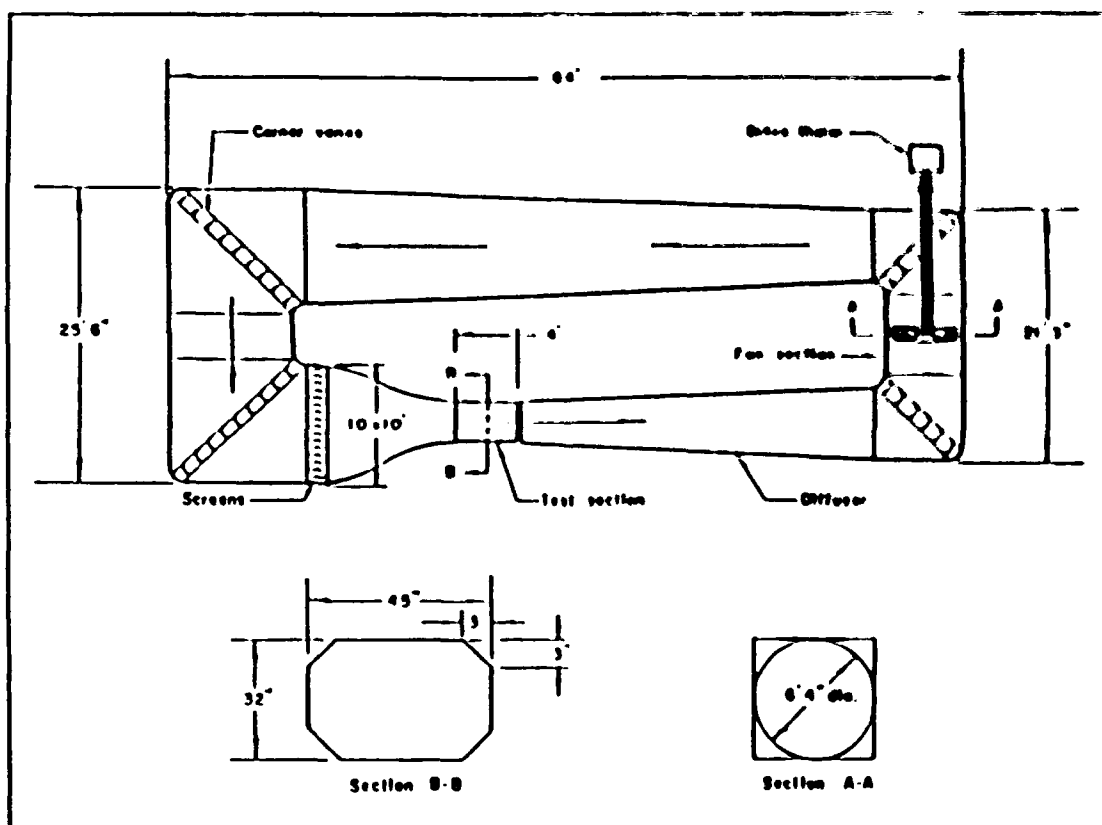


Figure 2. NPS Low-speed Wind Tunnel

Total length \approx 22.85 in.
 Base diameter \approx 1.75 in.
 Length/diameter ratio \approx 13.06
 Ogive nose length \approx 4.0 in.
 Ogive/diameter ratio \approx 2.29
 Wing span/root chord \approx 3.13 in./13.55 in.
 Tail span/root chord \approx 5.50 in./1.70 in.
 Center of pressure \approx 13.5 inches aft of nose tip (approx.)

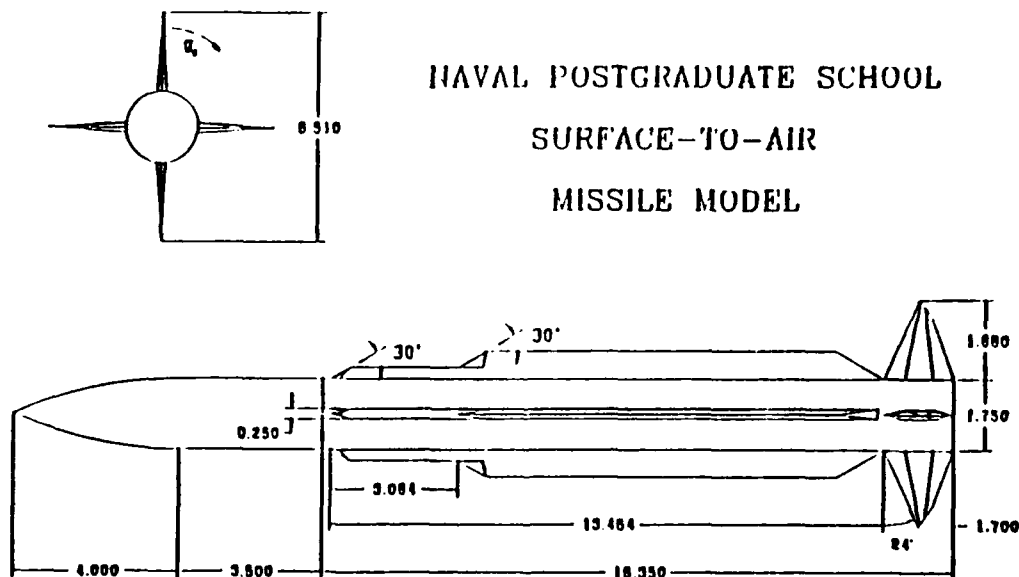


Figure 3. Missile Model Dimensions

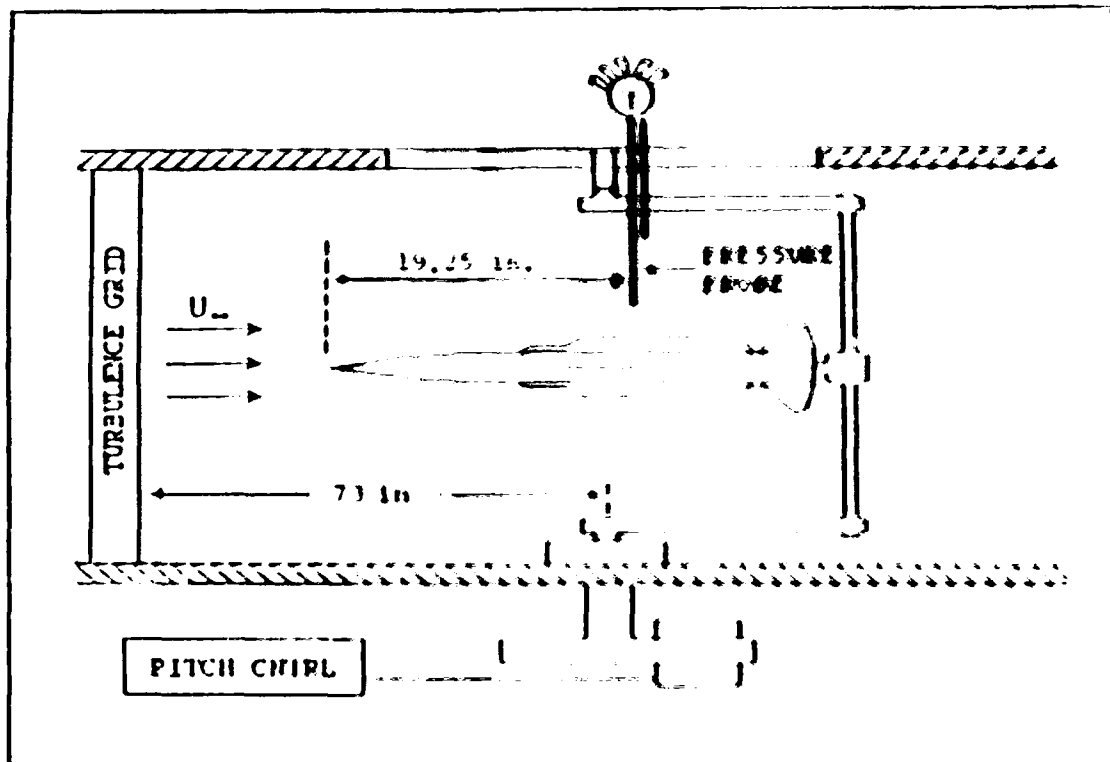


Figure 4. Mounting Arm Assembly

The three-axis traverser can be either manually or computer operated. It was mounted on the top of the wind tunnel. For the experiment the traverser was operated using software (PPROBE) modified by Lung. [Refs. 7, 16]

A five-hole pressure probe was mounted to the traverser and used to obtain pressure measurements at each data point. A portable manometer was used to measure the values of the P2 and P3 ports (static ports located on each side of the probe). By rotating the probe until these values were equal, the yaw

angle of the flow could be read directly from the probe. There are three ports in the front of the probe. One of the ports measures stagnation pressure. Located above and below it are two canted ports. Measurements from these are used with calibration curves to provide the pitch angle. Velocity was obtained by using the static and stagnation pressures and the calibration curves.

The data acquisition system consisted of a 48-port scanivalve attached to the probe and a Hewlett-Packard data acquisition system consisting of a relay multiplexer, digital multimeter, and relay actuator, and the software (PPROBE) required to operate the system [Refs. 7, 8, 17]. The scanivalve allows five pressures to be measured and converted to voltages by one transducer.

The data reduction/display software consisted of a FORTRAN program (CONVERT) written by Lung [Ref. 7]. The program was modified to be interactive, to include pitch and yaw corrections [Ref. 8], and to produce output required for this research. The program converted transducer voltages measured at each of the ports of the probe to pressures, velocities, and pressure coefficients using equations developed by Lung from the calibration data provided by the probe manufacturer [Refs. 7, 18]. Another FORTRAN program (VORTIC) was written to use the velocity components from CONVERT to compute

vorticity. A commercially-available graphics program was used to construct the various vector and contour plots.

C. SURVEY GRID

Figure 5 shows the location of the survey grid. It was perpendicular to the freestream flow at a location 11 missile diameters back from the missile nose (19.25 inches). The axis labeling coincides with the wind tunnel and not with the axis of the missile. After an initial survey of a 5-inch by 7-inch grid, an experimental survey grid size of 3.5 inches by 6 inches was decided upon, as it appeared to include the most significant information. Figure 6 shows the survey grid dimensions. The grid started .75 inches away from the missile wing and 3 inches below the center line. The top and bottom areas near the missile were not surveyed because of interference between the sting mounting arm and the probe. The same starting point and grid size were used for both roll angles. By using a data point spacing of .25 inches, data were taken at a total of 367 positions for the OA configuration and 369 positions for the other three configurations.

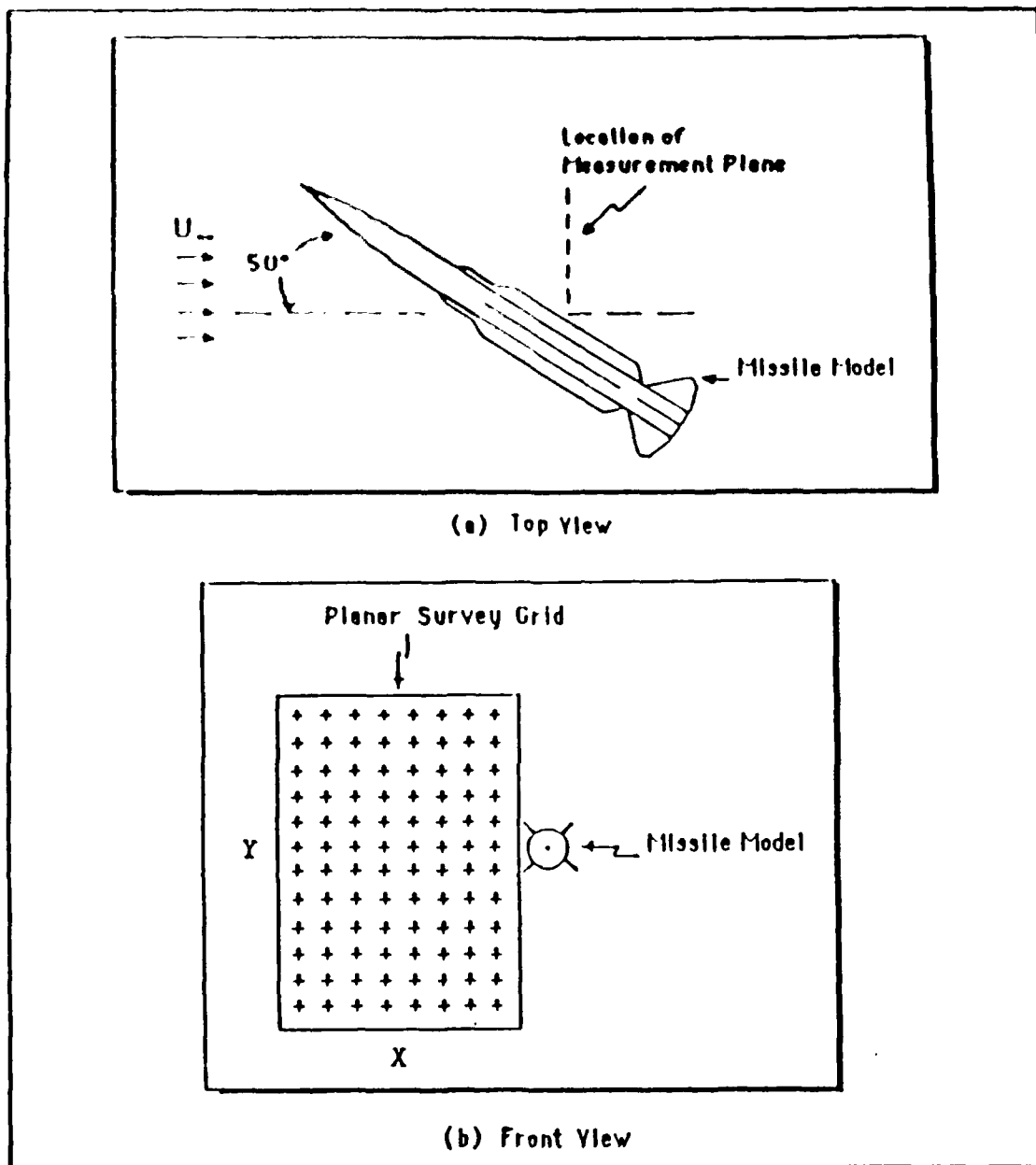


Figure 5. Survey Grid Location

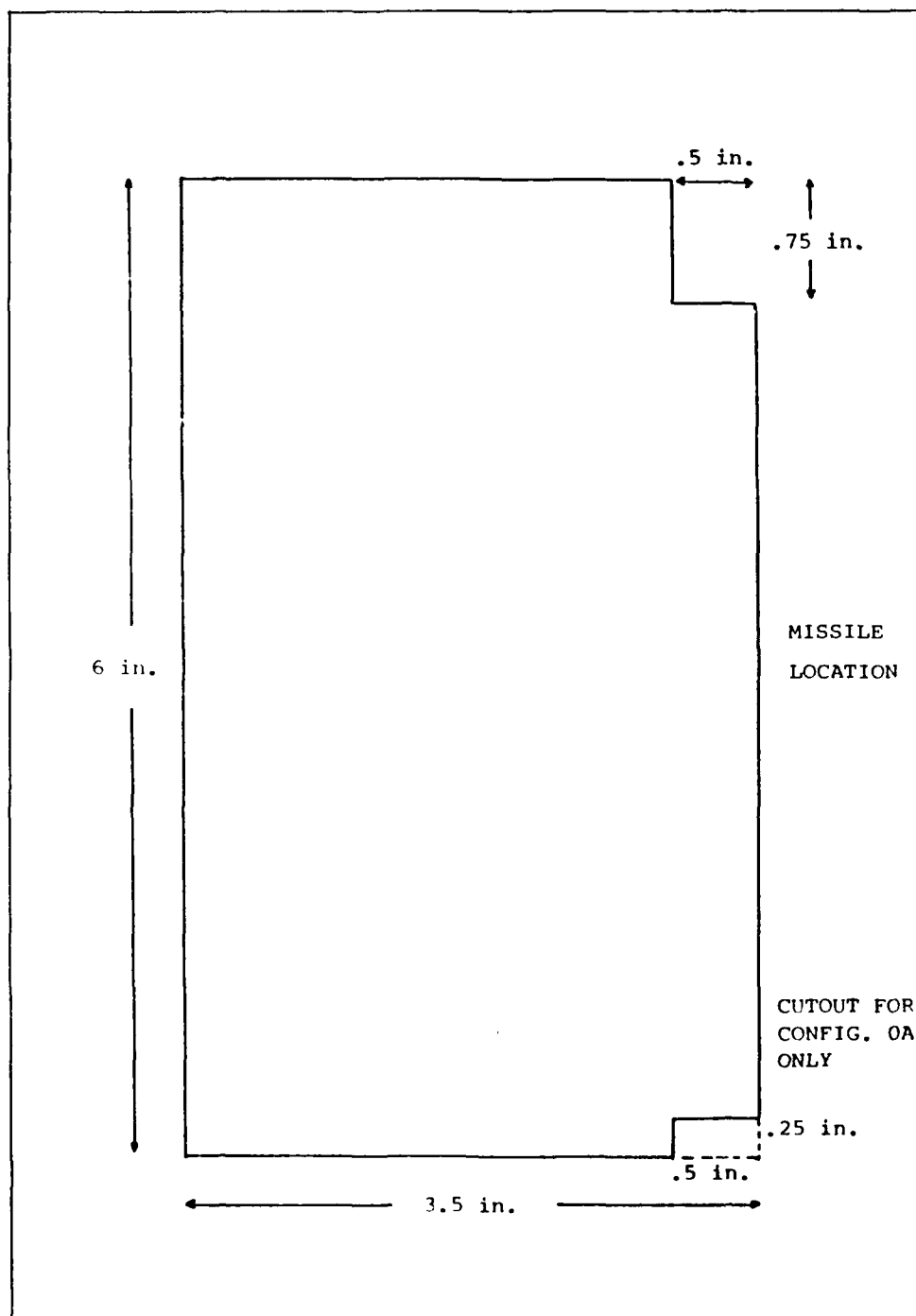


Figure 6. Survey Grid Dimensions

D. TEST CONDITIONS

In order to facilitate data correlation with previous research done by Rabang [Ref. 10], Lung [Ref. 7], and Viniotis [Ref. 8], the following experimental conditions were used.

(1) A Reynolds number of 1.1×10^5 was maintained by using a reference pressure of 7.2 cm H₂O during data acquisition with no turbulence grid and 10.0 cm H₂O with the turbulence grid. These settings were determined by Roane [Ref. 11] and insured that the test section velocity was the same for each of the configurations. It also ensured that the turbulence grid produced the same length scale and intensity as used in previous research.

(2) Turbulence grid #3 was used to introduce turbulence into the freestream. Rabang [Ref. 10] noted that grid #3 produced vortex-length-scale turbulence and had the largest effect on the side force on the missile.

(3) The nose roll angle was set at nose position eight. Rabang [Ref. 10] determined that nose roll angle affected the forces and moments and position eight produced the largest forces for this missile model.

(4) Measurements were taken with the missile at two roll angles, 0 degrees (the body in a "+" configuration) and 45 degrees (the body in an "x" configuration).

(5) The missile angle of attack was fixed at 50 degrees which Rabang [Ref. 10] determined as the position for maximum side force.

(6) The data plane was located 11d (19.25 inches) back from the nose (versus 6d or 10.5 inches used by Lung and Viniotis).

(7) Wind tunnel temperatures were not allowed to vary by more than 20 degrees during a data acquisition run. When using the turbulence generating grid, the temperature would increase by this amount in approximately one hour. When the limit was reached, the measurement process was stopped, the tunnel velocity was slowed, and air exchange doors were opened until the temperature cooled. Measuring was then resumed.

E. EXPERIMENTAL VARIABLES

The pressure measurements were converted to characteristic variables of the vortices using CONVERT, a FORTRAN program (Appendix A). The variables were velocities (total, x and y components), pitch angle, total pressure and its coefficient, static pressure and its coefficient, and vorticity. Yaw angle was read directly from the probe.

Velocities, pitch angle, and pressures were computed using calibration curves from the probe manufacturer [Ref. 18].

The pressure coefficients were computed using the room ambient pressure as the reference and non-dimensionalized by the tunnel dynamic pressure.

$$C_{PS} = (P_{sL} - P_R) / Q \quad (1)$$

$$C_{PT} = (P_{tL} - P_R) / Q \quad (2)$$

where

C_{PS} = Static pressure coefficient

C_{PT} = Total pressure coefficient

Q = Freestream dynamic pressure

P_R = Reference pressure (equal to ambient pressure)

P_{sL} = Local static pressure

P_{tL} = Local total pressure

Vorticity was computed by the program VORTIC (Appendix B) using Equation 3 and a numerical differencing scheme to compute the partial derivatives.

$$V = \partial v / \partial x - \partial u / \partial y \quad (3)$$

V = Vorticity

v = y component of the velocity

x = x distance

u = x component of the velocity

y = y distance

F. PROCEDURE

The procedure for gathering the data was as follows.

(1) The data acquisition equipment was turned on and allowed to warm up for approximately ten minutes. During this time ambient temperature and pressure were recorded.

(2) The CALP program was used to calibrate the transducer attached to the scanivalve.

(3) Using the manual option of the PPROBE program, the probe was positioned so the stagnation port was level with the edge of the wing. It was then moved down half of the y-dimension (3 inches). Using the computer-controlled option, the survey grid size was entered into the program and the data gathering was controlled by the program. The program prompts for input of the yaw angle. The probe was manually turned until the difference between the P2 and P3 values was approximately zero. The yaw angle was read directly from the probe and entered. The program then stepped through each of the five pressure ports, taking ten measurements at each. The average time to take the five measurements was 20 seconds. The measurements were averaged by the program for the data point. In order to ensure that the probe was facing the proper direction, the P1 measurement had to be a positive value or a very small ($>-.5$) value. If the difference between P2 and P3 were not within .1 volts or P1 was not

acceptable, the probe would be realigned and data for that point would be remeasured. At the end of one column of data (the y direction) the x-y position and the five average voltages for each data point would be recorded on a floppy disk.

(4) At the end of the data acquisition, the CALP program was run again. This allowed the transducer calibration data to be averaged because it would have small changes during the data acquisition run (the runs took approximately eight hours). The calibration data (voltage versus pressure) was used to develop a calibration curve. The slope and intercept for the curve were used in the CONVERT program.

(5) The CONVERT program (Appendix A) was used to convert the voltages at each point into velocity and pressure data. The program is interactive and asks for various initial and final wind tunnel conditions, slope and intercept determined from the CALP program, reference dynamic pressure, and wind tunnel calibration factors. [Refs. 7, 8, 10, 11]

(6) The VORTIC program (Appendix B) used velocity output from CONVERT to compute the vorticity at each point using a numerical differencing scheme.

(7) After changing the output files from CONVERT and VORTIC to the input format required by the graphics plotting software, velocity vectors and contours for total pressure coefficient, static pressure coefficient, and vorticity were plotted.

III. RESULTS

A. INTRODUCTION

The results of the study will be presented in four sections, representing the four sets of experimental conditions. The sequence will be results with wings in the "+" configuration without the turbulence grid (0A), wings in the "+" configuration with the turbulence grid (3A), wings in the "x" configuration without the turbulence grid (0C), and wings in the "x" configuration with the turbulence grid (3C). For each condition, the order for the results will be velocity vector plots, total pressure coefficient contour plots, and vorticity contour plots (including plots from Viniotis [Ref. 8] for comparison). The plots from Viniotis are at a survey plane 6d (10.5 inches) back from the missile nose. Static pressure contour plots are included for completeness in Appendix C.

The plots show the missile as it appeared in the tunnel when viewed in the direction of the tunnel freestream. All measurements are in missile diameters (1.75 inches) and will be from the leeward side of missile body and the centerline. Reference above and below the centerline are left and right of the missile axis when viewed in the direction of the freestream in flight.

B. CONFIGURATION 0A

Figures 7, 8, and 9 have a space (void) in the grid pattern where data could not be obtained because of limitations in the pitch angle measurement range of the probe.

The velocity plot (Figure 7) shows the location of one vortex and indicates the location of another. The velocity vectors show the opposite rotation of the flow. The vectors along the center line all show the asymmetry of the flow. They all have components downward and do not flow directly at the missile. The location of the lower vortex is well defined. The upper vortex location can be assumed to be located in the vicinity of the void, near the edge of the survey pattern because of the changing length and direction of the vectors.

The total pressure plot (Figure 8) shows centers of large losses. The first is approximately $1.03d$ below and $1.91d$ away. The second is assumed to be located in the void, approximately $.91d$ above and $1.34d$ away. The centers of loss coincide with the core defined by the velocity vectors, although the areas are larger than the cores.

The vorticity plot (Figure 9) shows two main patterns of vorticity. The contour line labeled 4 is approximately the zero value. Values below 4 indicate rotation in one direction, values above indicate rotation in the other. The

upper portion of the plot shows a high positive value of vorticity .69d above and 2.37d away. There also appears to be a high value close to the edge of the survey grid although the vorticity values in the void cannot be easily interpolated from the contour lines. There are two centers of high negative vorticity in the lower portion. One is located 1.03d below and 2.6d away and the other is 1.14d below and 1.06d away. Both have approximately the same magnitude as the upper values. The areas of greatest vorticity magnitude are not in the same location as the vortex core from the velocity vectors and the largest pressure losses.

The vorticity plot from Viniotis (Figure 10) shows two very well defined patterns of vorticity. The centers are asymmetric with the lower one being farther down but closer to the body. Although the magnitudes are approximately the same, the upper one appears to be stronger due to the larger gradient. At the edge of the survey grid nearest the missile, there are indications of two smaller, stronger vortices. Comparing the vorticity plots, it appears that the large well defined centers and the smaller stronger centers on Viniotis' plot move away from the missile and move farther apart from each other, as indicated by the four centers on the vorticity plot. As the centers move back along the missile, the values of vorticity in the upper areas decrease while the lower areas' values are approximately the same.

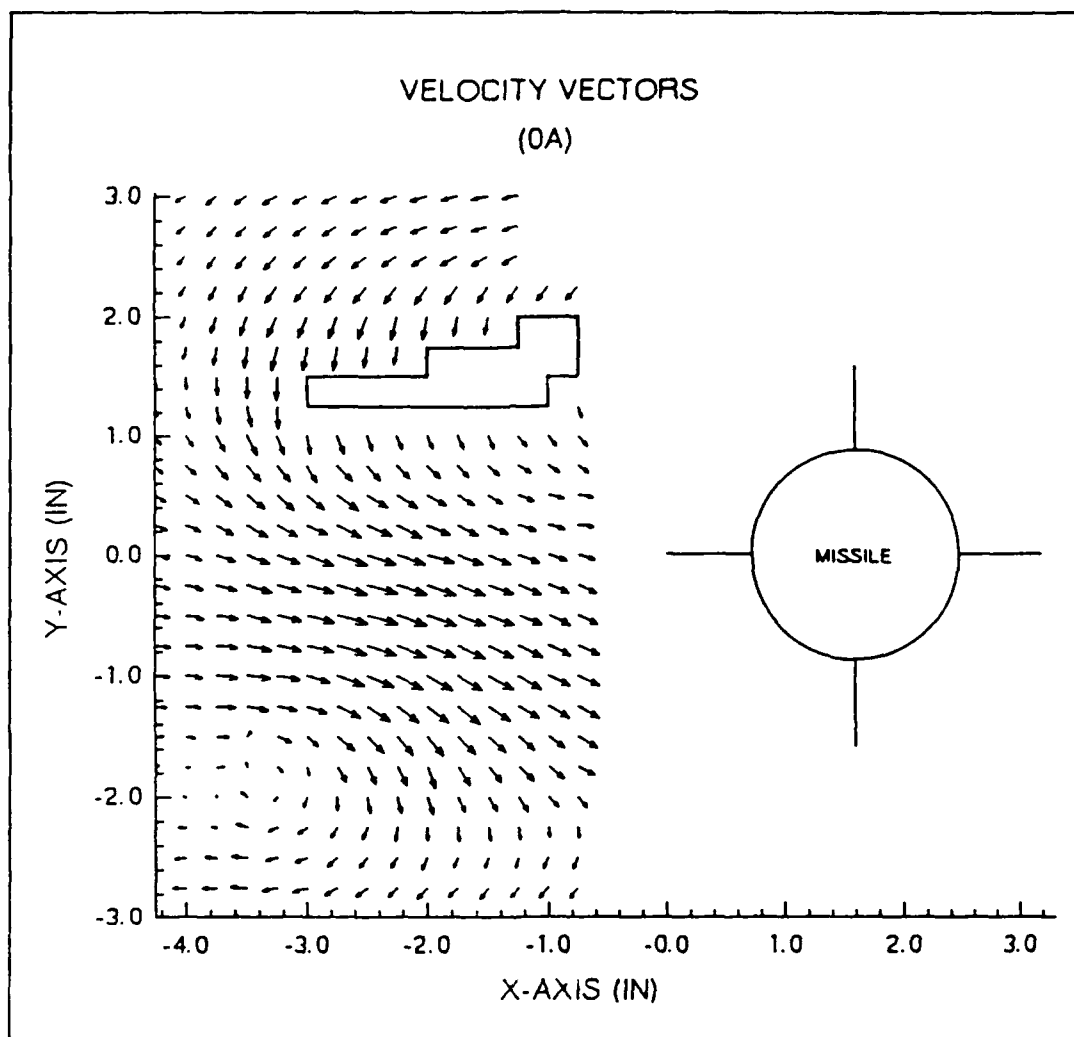


Figure 7. Velocity Vectors - Configuration 0A

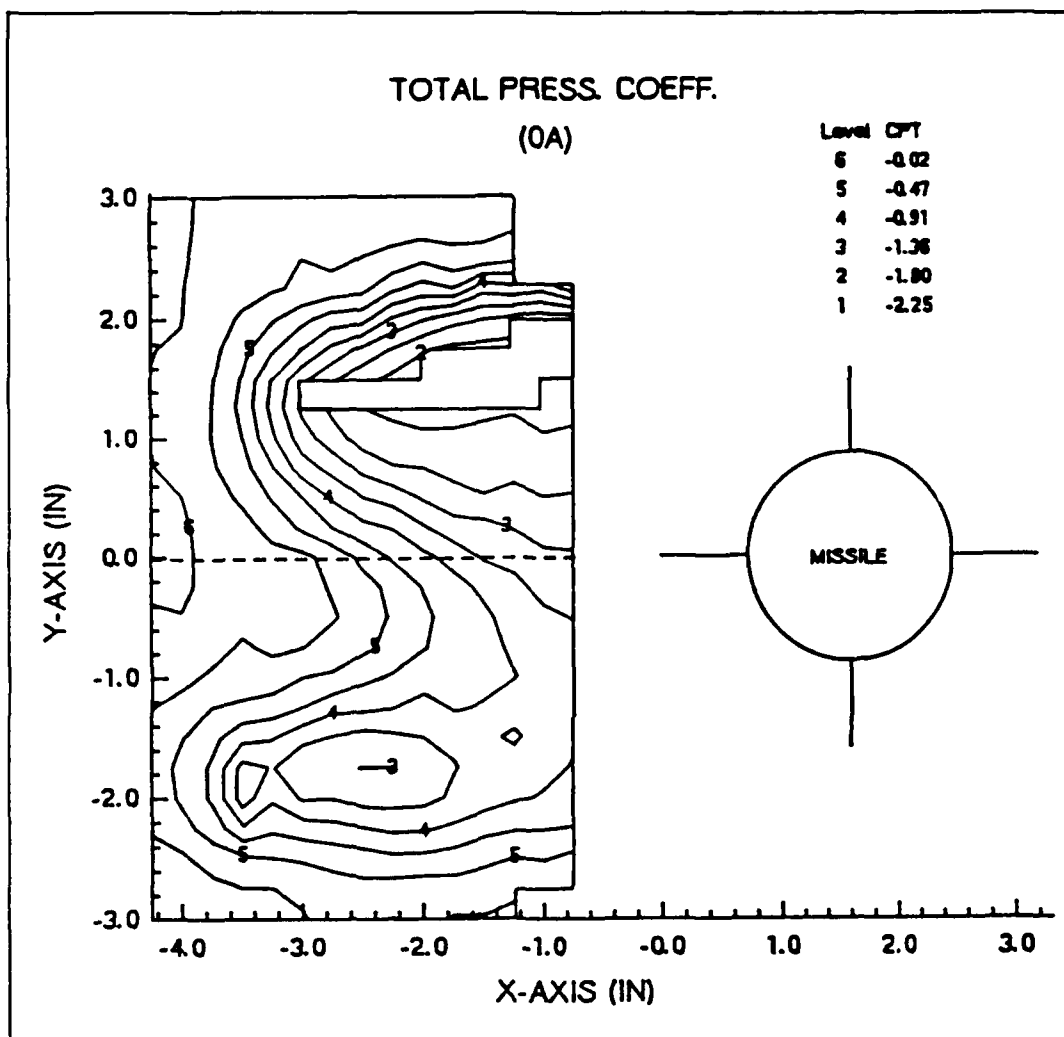


Figure 8. Total Pressure Coefficient - Configuration 0A

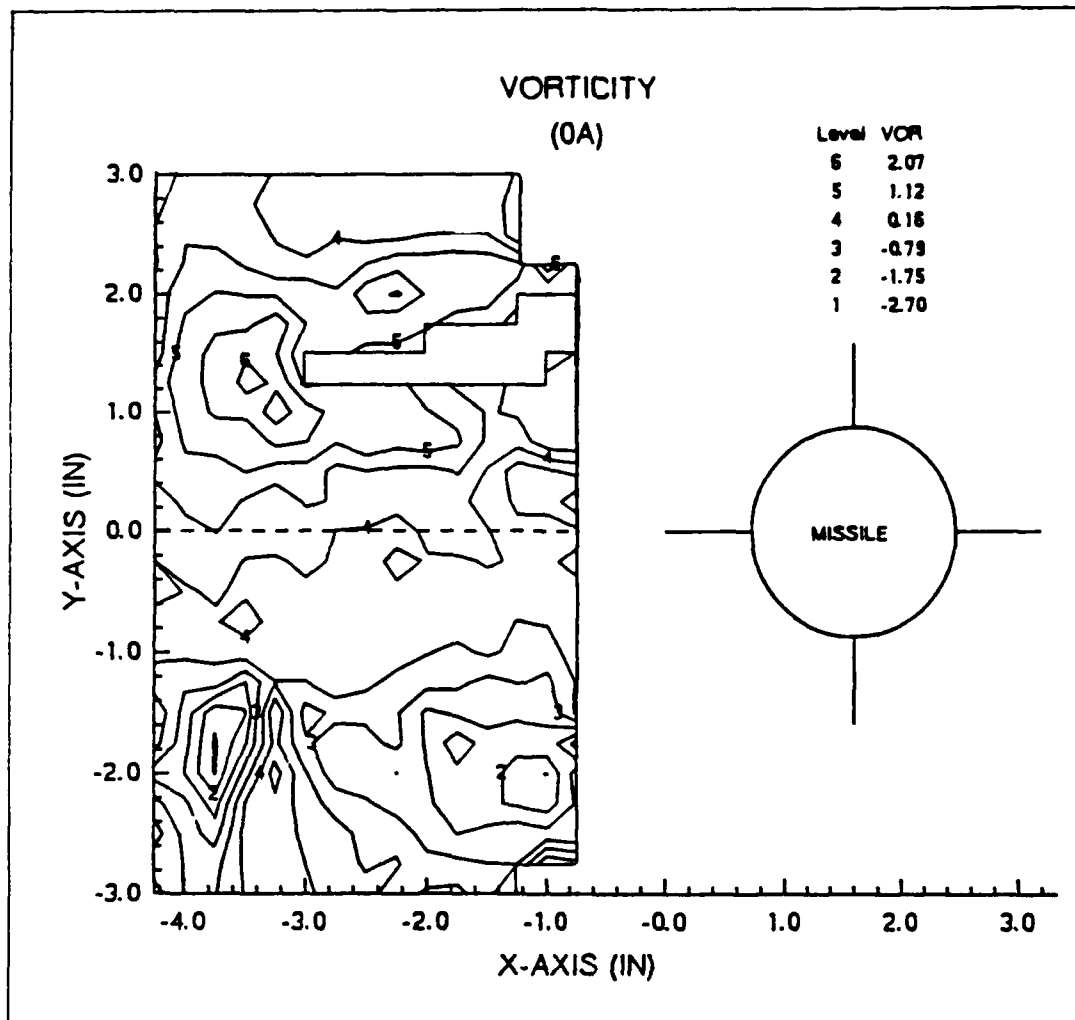


Figure 9. Vorticity - Configuration 0A

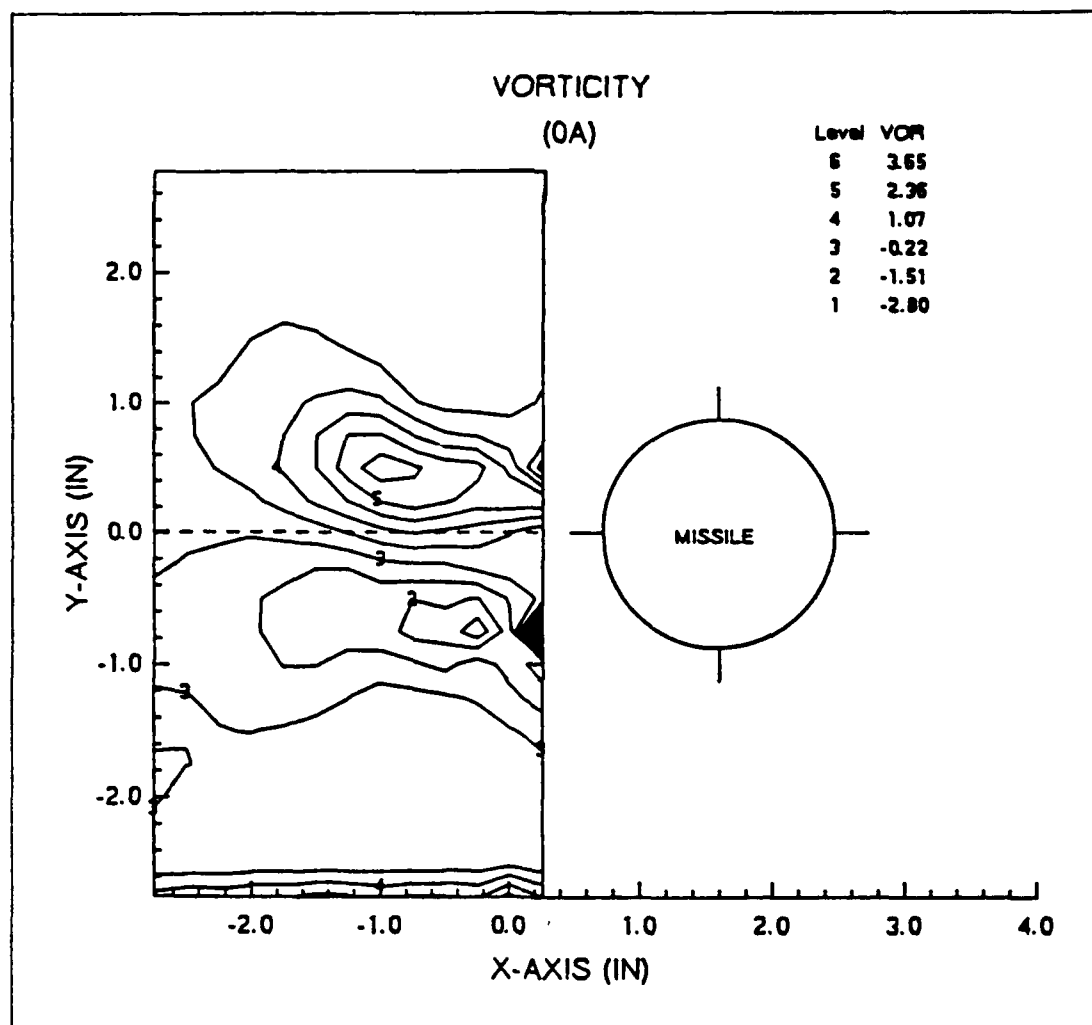


Figure 10. Vorticity (at 6d) - Configuration 0A

C. CONFIGURATION 3A

This configuration differs from the 0A configuration only in the addition of the turbulence generating grid. Figures 11, 12, and 13 have a space (void) in the grid pattern where data could not be obtained because of limitations in the pitch angle measurement range of the probe, although the area is smaller than the 0A configuration.

The velocity plot (Figure 11) shows the location of one of the asymmetric vortices and indicates the location of the other. The vortices are rotating in opposite directions. The lower one is $1.14d$ below and $2.43d$ away. The upper one appears to be located in the vicinity of the void and the edge of the survey grid.

The total pressure plot (Figure 12) shows two centers of losses. One is $1.03d$ below and $1.69d$ away. The other appears to be centered in the void, $.86d$ above and $1.11d$ away. The upper center has a larger gradient, with the losses concentrated in a smaller area. The location of the upper center coincides with the core as shown by the velocity vectors. The lower center does not coincide with the lower core shown by the velocity vectors, indicating that the vortex core is not the location of greatest losses in the flow.

The vorticity plot (Figure 13) indicates four centers of magnitude peaks, with the zero value being approximately $.57d$

below centerline. The two lower centers appear to be at the edges of the survey grid, 1.03d below and 2.86d away and 1.14d below and .86d away. One upper center is well defined .69d above and 2.14d away. The other appears to be in the void, .8d above and 1d away. The upper center closest to the missile coincides with the centers shown by the velocity and pressure plots. The lower centers do not coincide with either of the other plots. Apparently the vorticity has become very diffused for the vortex located farther from the missile.

The vorticity plot from Viniotis (Figure 14) shows two well-defined centers and indicates two others. The upper ones are .23d above and .86d away and .29d above and .43d away. The first one has a larger magnitude and gradient than the lower ones. The lower ones are located .46d below and .86d away and .57d below and .43d away. As the centers move downstream, the four centers move away from the centerline and the missile body. The magnitudes of all of the centers appear to decrease and the centers are more diffuse.

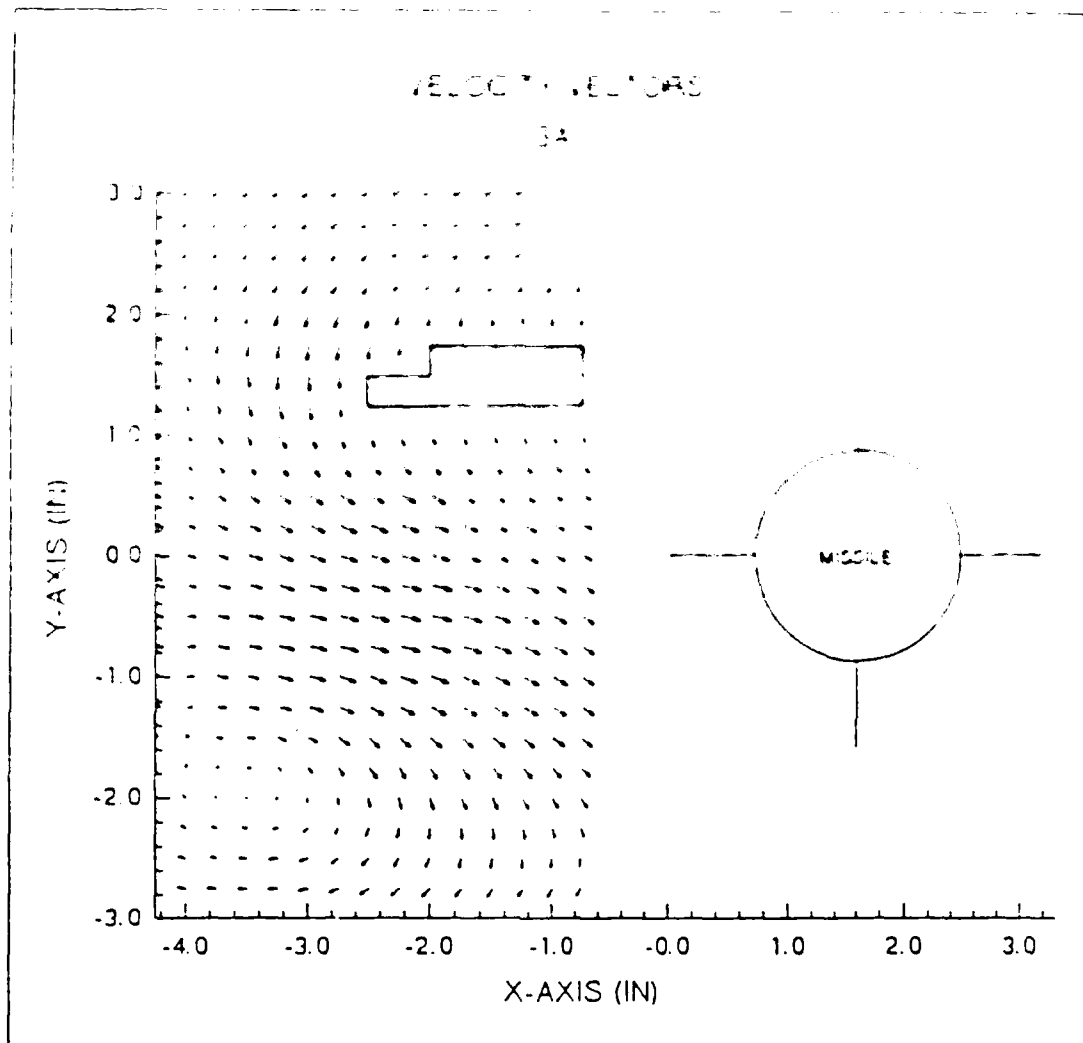


Figure 11. Velocity Vectors - Configuration 3A

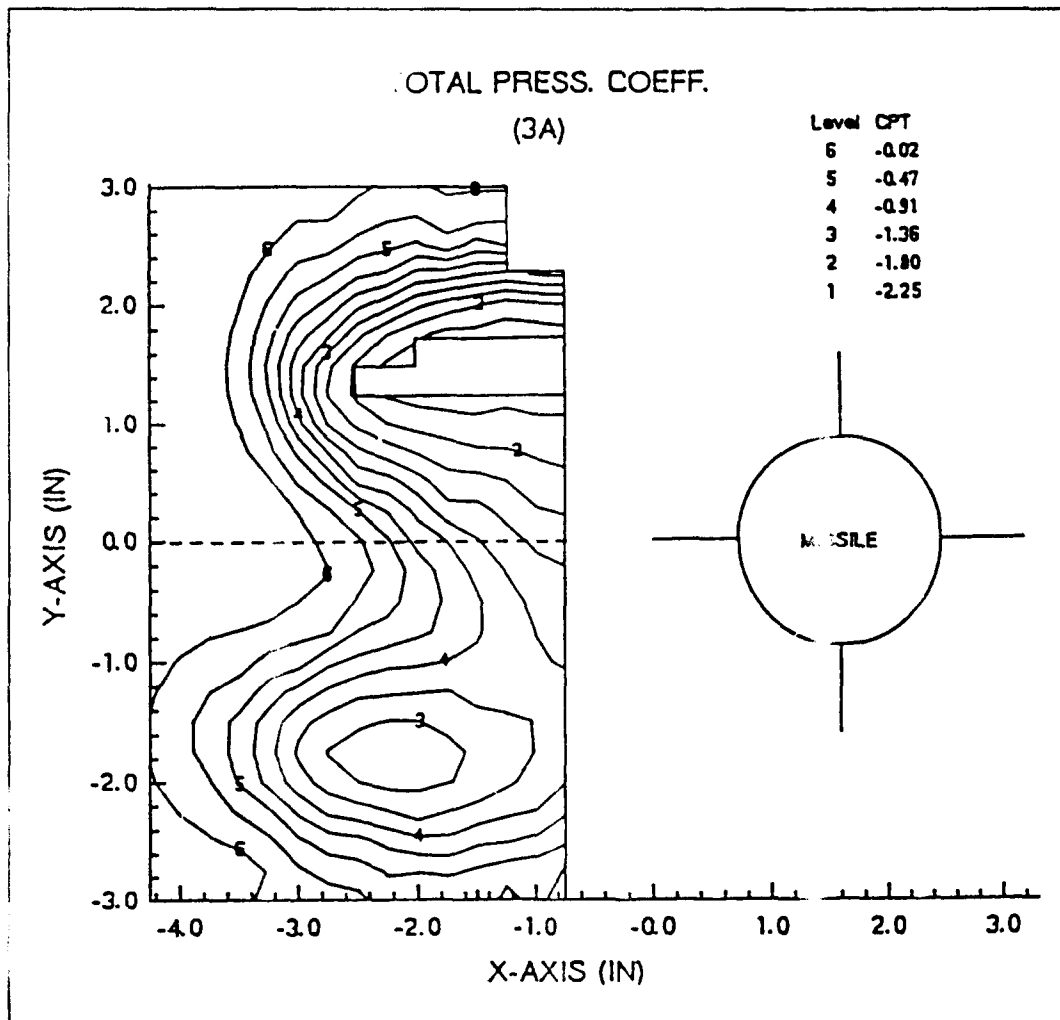


Figure 12. Total Pressure Coefficient - Configuration 3A

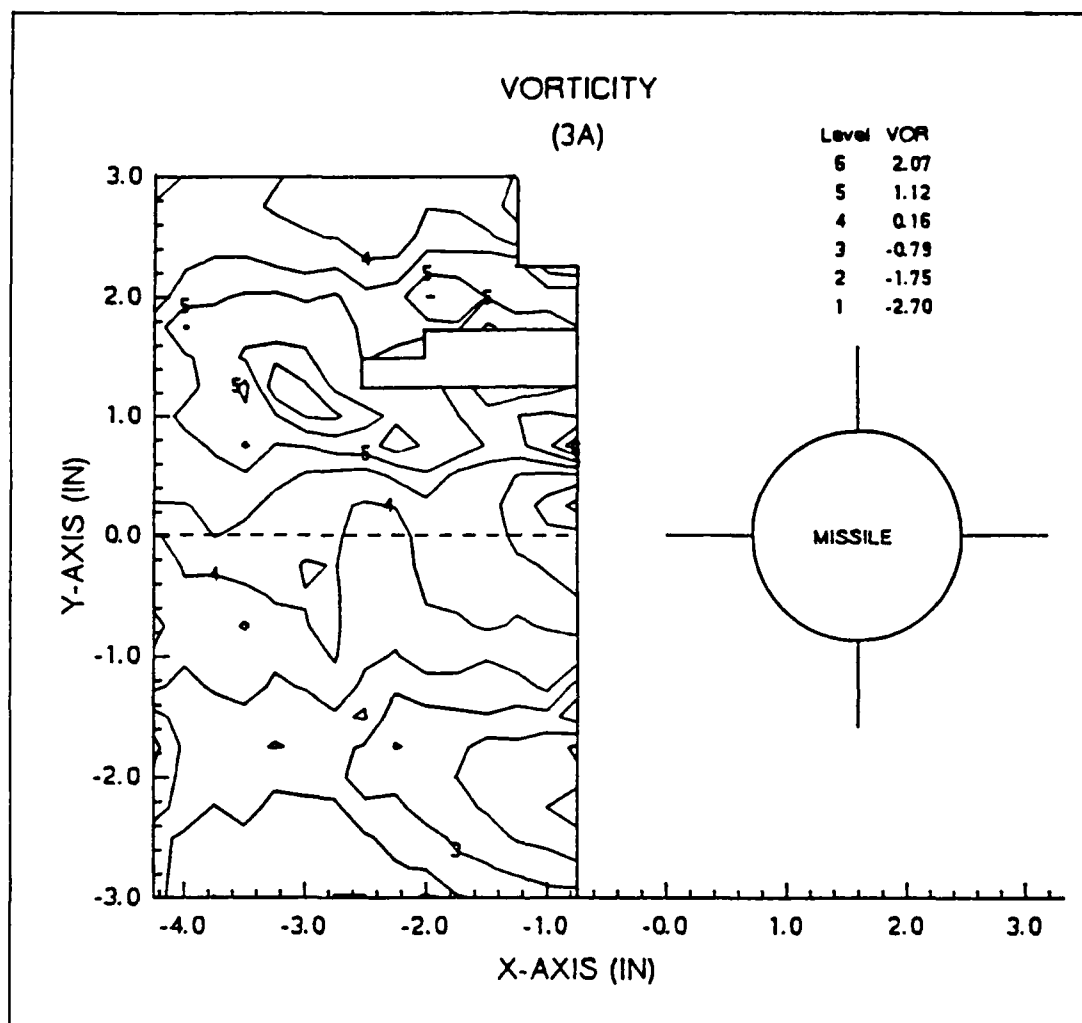


Figure 13. Vorticity - Configuration 3A

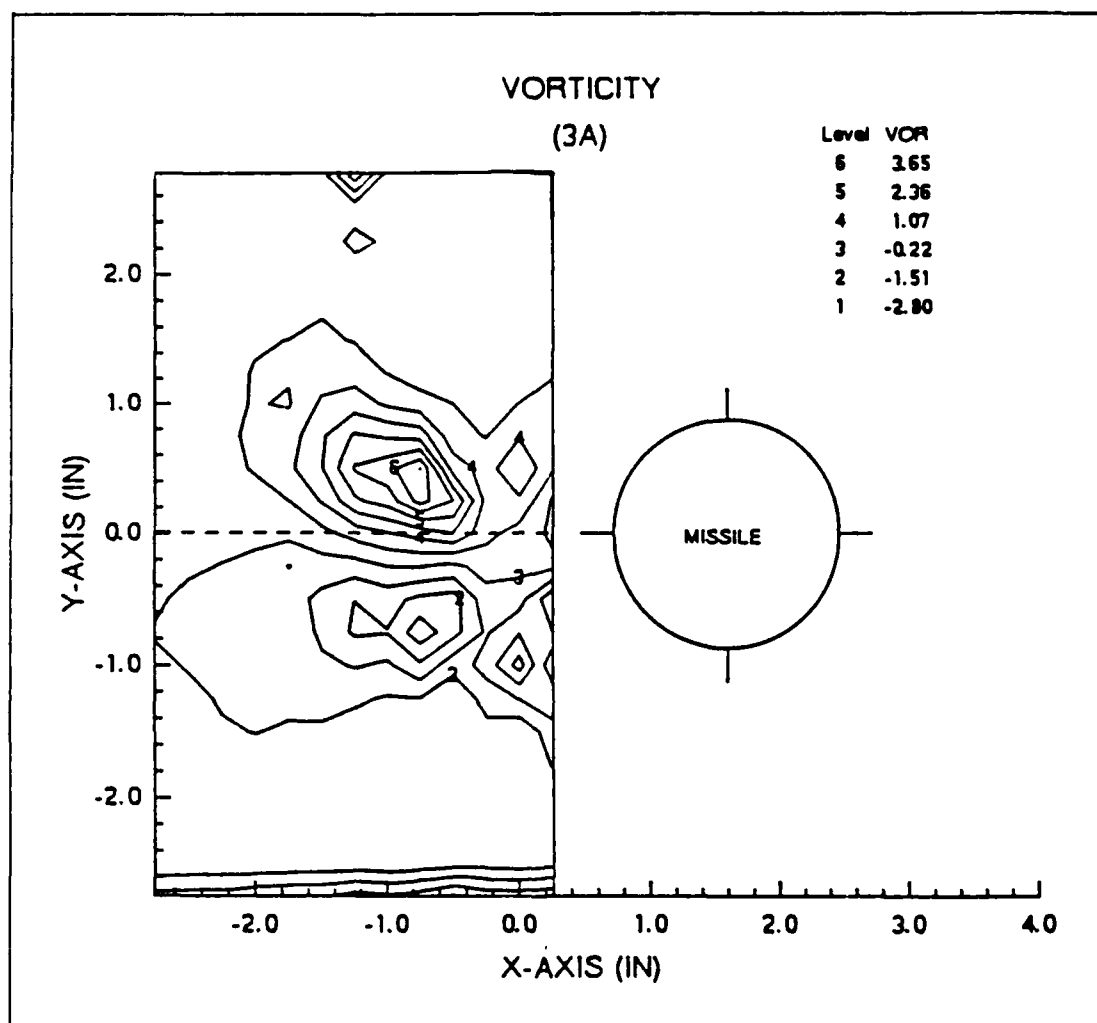


Figure 14. Vorticity (at 6d) - Configuration 3A

D. CONFIGURATION 0C

The change in the wing roll angle caused large changes in shapes of all of the plots. The entire flowfield was different from those of the "+" configurations.

The velocity plot (Figure 15) indicates the location of three vortices, one above centerline and two below. The upper one is located near the edge of the survey grid, .69d above and .86d away. The lower two are located at each end of the survey grid. One is .8d below and 2.86d away and the other is .69d below and .86d away.

The total pressure plot (Figure 16) shows one large center of loss, .23d above and 1.69d away. The center does follow the general pattern of the velocity vectors, although the center does not coincide with the core from the velocity vectors.

The vorticity plot shows (Figure 17) two centers and indicates two others at the edge of the survey grid. The zero value lies roughly along the centerline. The largest upper one is .29d above and 1.71d away. The next largest appears at the edge of the survey grid, .8d above and .86d away. There appears to be a small core .29d above and 1.43d away. This may be part of the well-defined center but appears separately due to the resolution of the survey grid. The lower centers are more diffuse and have less magnitude. They

are located $.63d$ below and $1.71d$ away and $.29d$ below and $.86d$ away. The location of the area of greatest vorticity coincides with the center of the pressure contours.

The vorticity plot from Viniotis (Figure 18) shows two centers. The upper one is $.17d$ above and $1.11d$ away. It has the highest magnitude and also the largest gradient. The lower one is $.43d$ below and $1.11d$ away. There also appears to be two centers at the edge of the survey grid, above and below centerline. The centers move farther away from the missile as they move along the missile. The strength in the upper center decreases while the strength in the lower is approximately the same. The areas are more diffused at the $11d$ survey grid location.

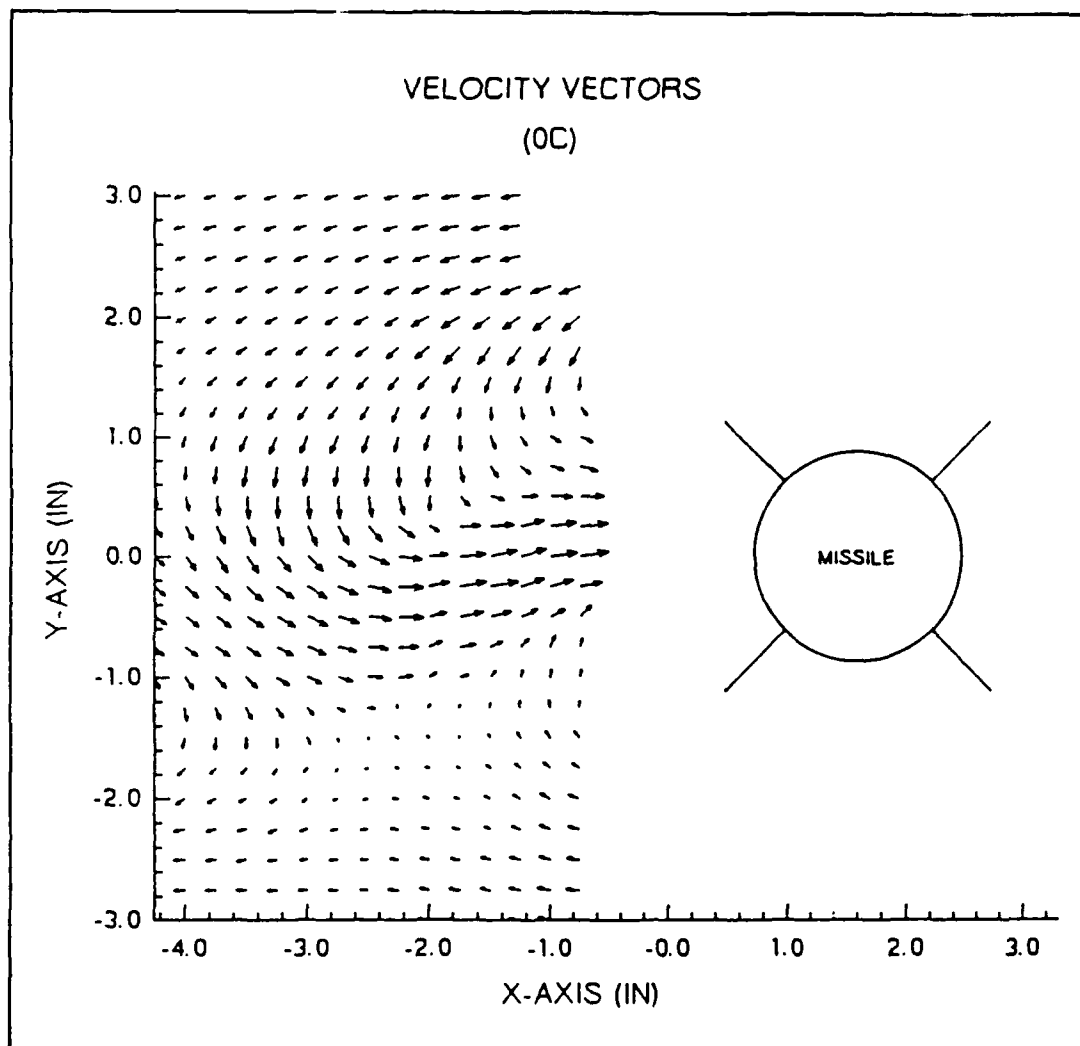


Figure 15. Velocity Vectors - Configuration 0C

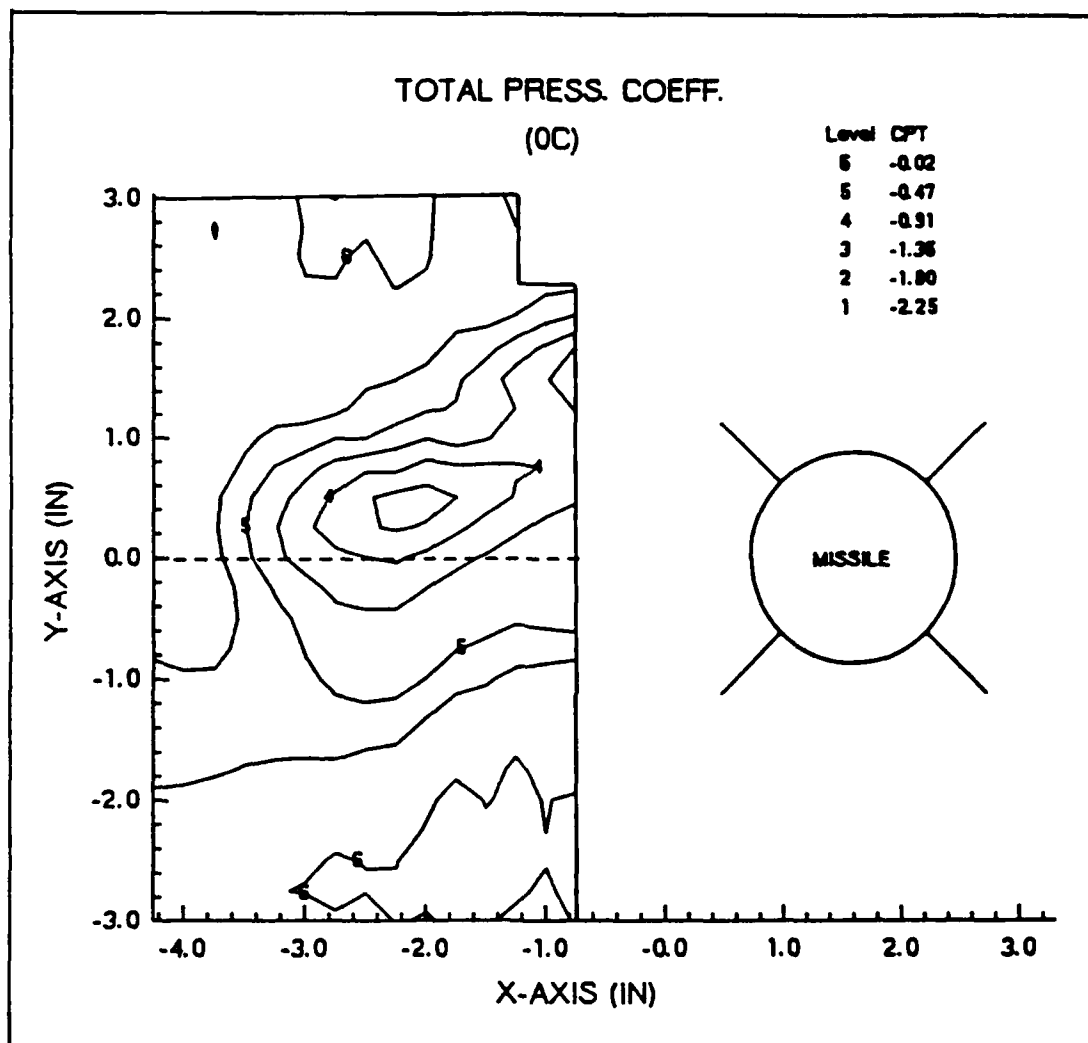


Figure 16. Total Pressure Coefficient - Configuration 0C

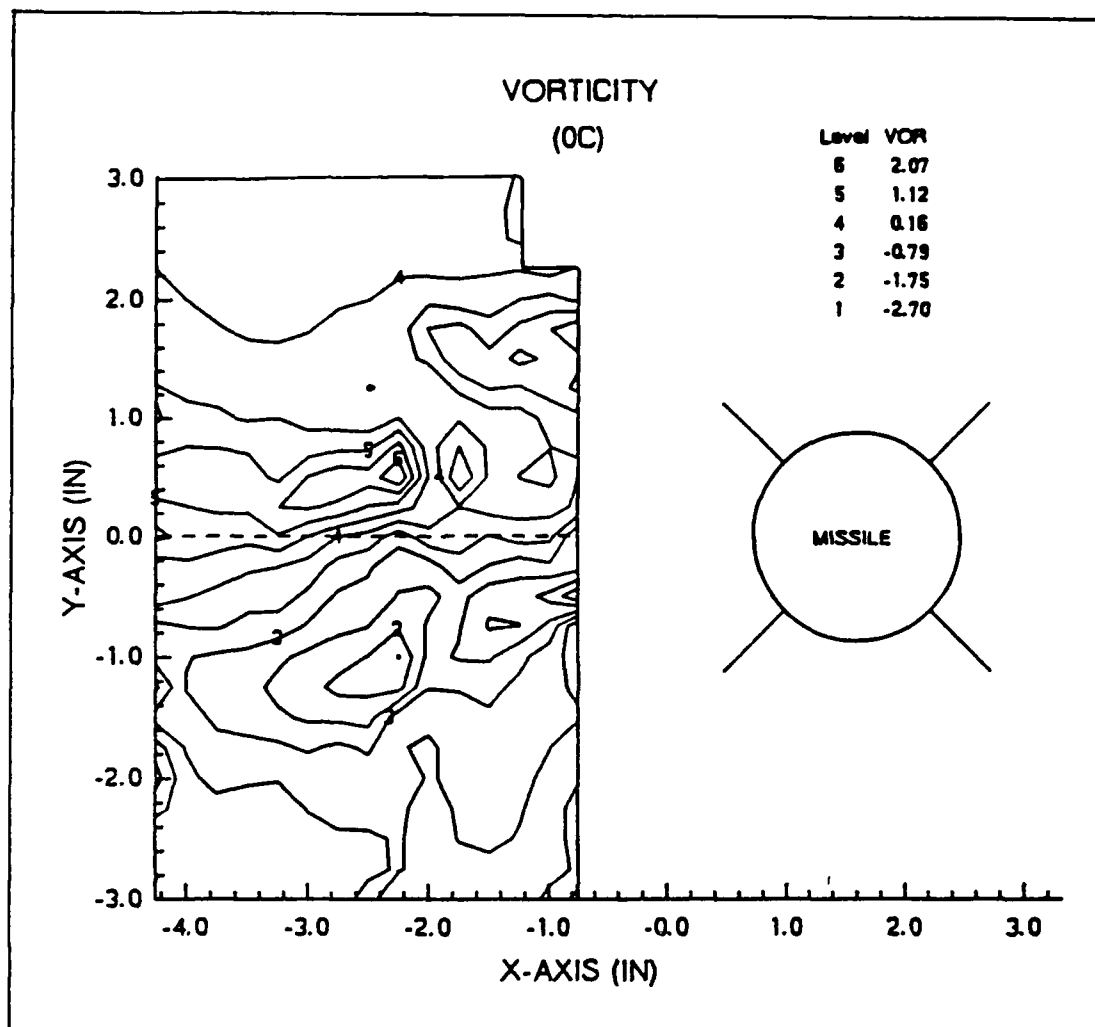


Figure 17. Vorticity - Configuration OC

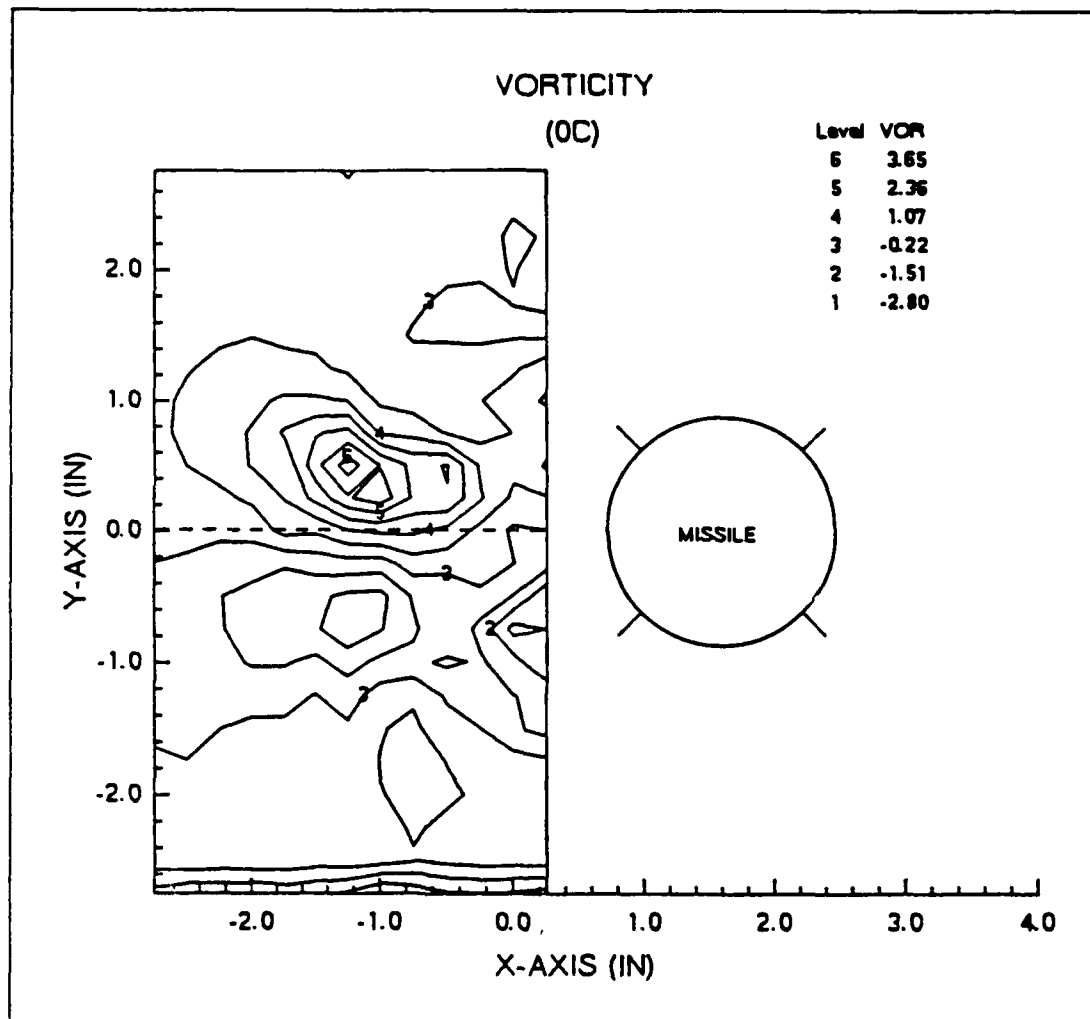


Figure 18. Vorticity (at 6d) - Configuration OC

E. CONFIGURATION 3C

The addition of turbulence did not have a large effect on the patterns in the data plots for this configuration.

The velocity plot (Figure 19) indicates the location of three vortices. All of them are located at the edges of or outside of the survey grid. The upper one appears to be located $.69d$ above and $.86d$ away. The lower ones appear to be located $.8d$ below and $2.86d$ away and $.69d$ below and $.86d$ away.

The total pressure plot (Figure 20) shows one large center located $.23d$ above and $1.8d$ away. As with the 0C configuration, the area follows the general pattern of the velocity vectors, although the center of the area does not coincide with the core from the velocity vectors.

The vorticity plot (Figure 21) shows two centers. The zero value is approximately along the centerline. The upper center is $.29d$ above and $2.09d$ away. Another center may be located at the edge of the survey grid, $.8d$ above and $.86d$ away. The lower one has less magnitude and is more diffuse and with the center located $.57d$ below and from $.86d$ to $2.09d$ away. The center of the upper area coincides with the center in the pressure plot.

The vorticity plot from Viniotis (Figure 22) shows two centers. The upper one is $.29d$ above and $1.11d$ away. The

lower one is $.46d$ below and $.29d$ away. The centers have the same magnitude and approximately the same gradient. The lower center is more diffuse (elongated) than the upper one. As the centers move back along the missile, the largest magnitude of the vorticity decreases and the centers are more diffuse.

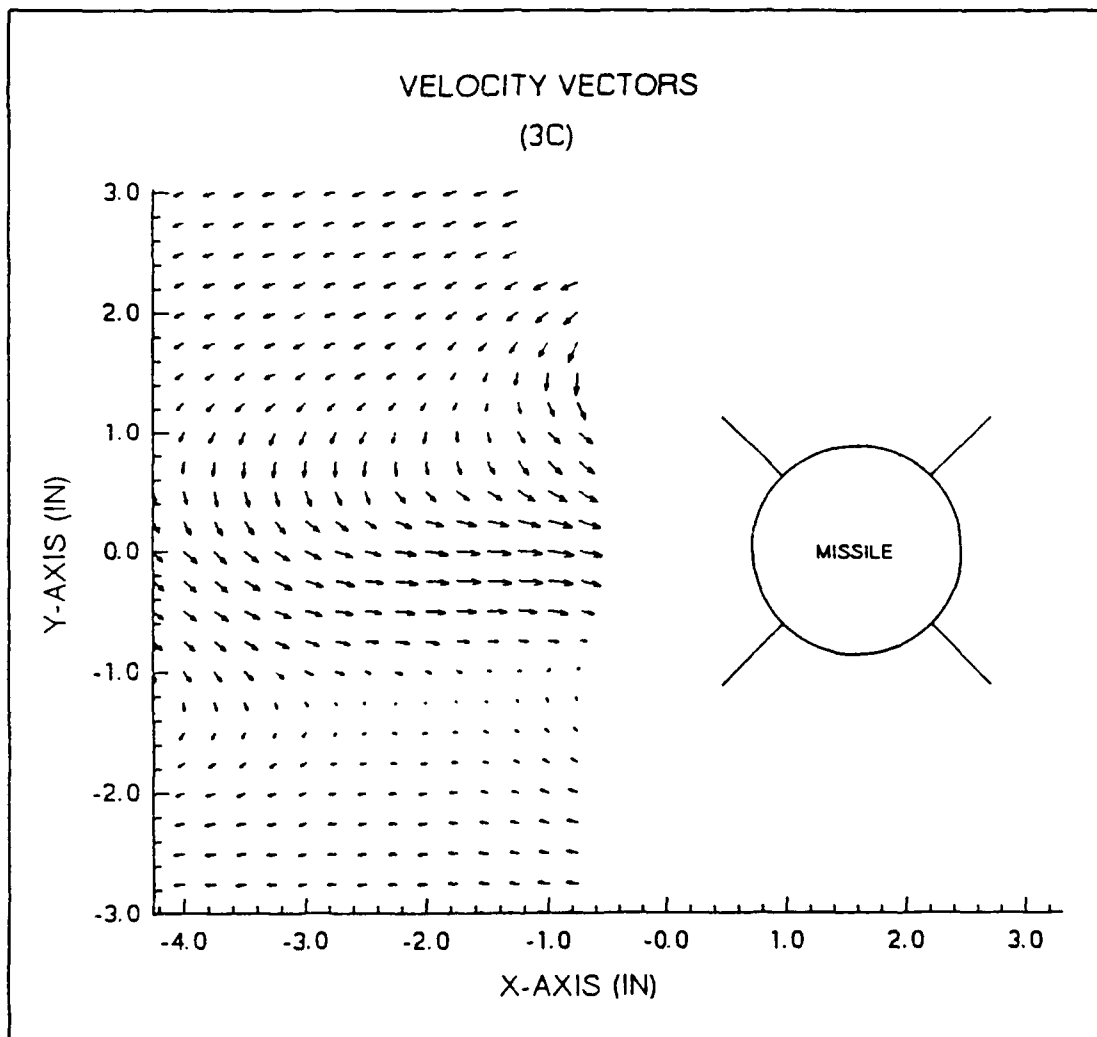


Figure 19. Velocity Vectors - Configuration 3C

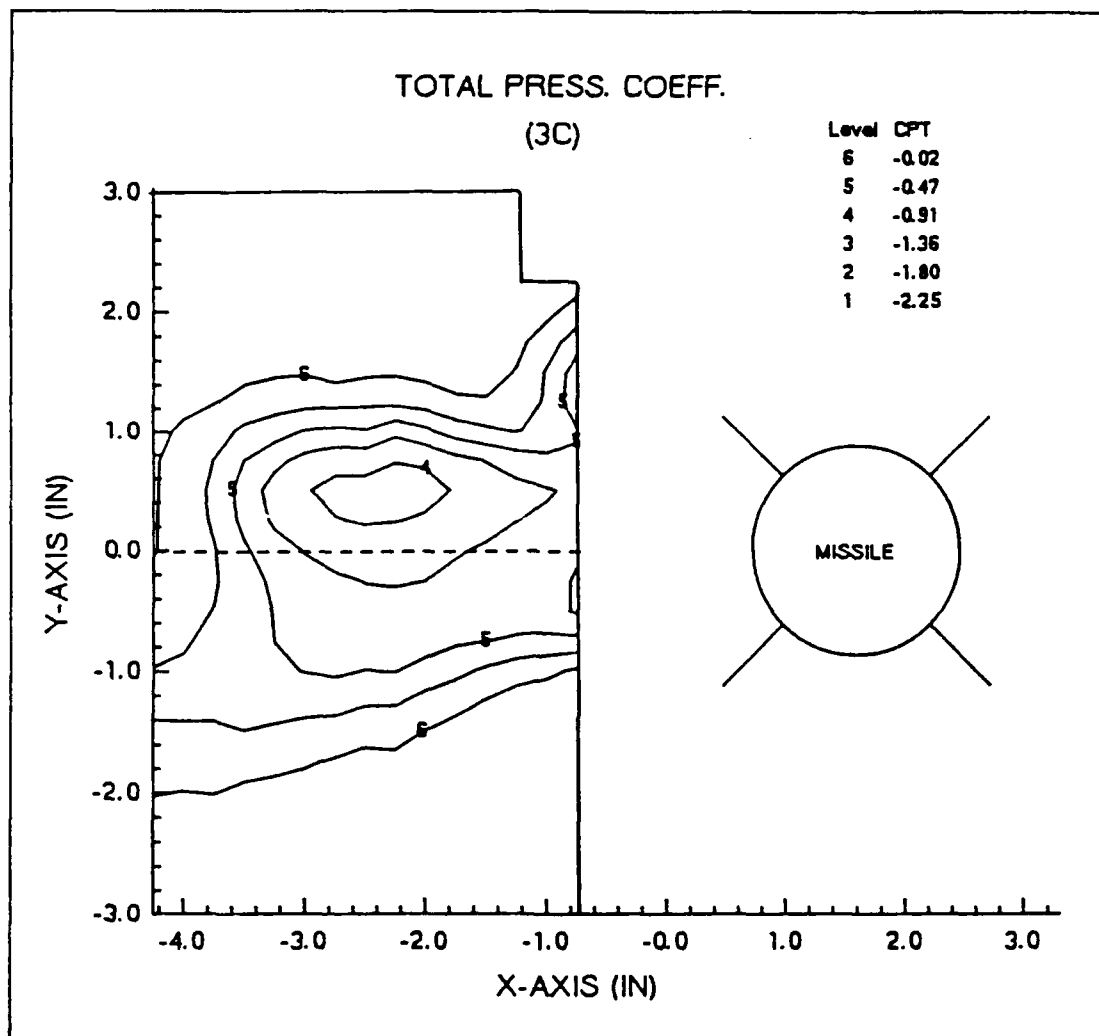


Figure 20. Total Pressure Coefficient - Configuration 3C

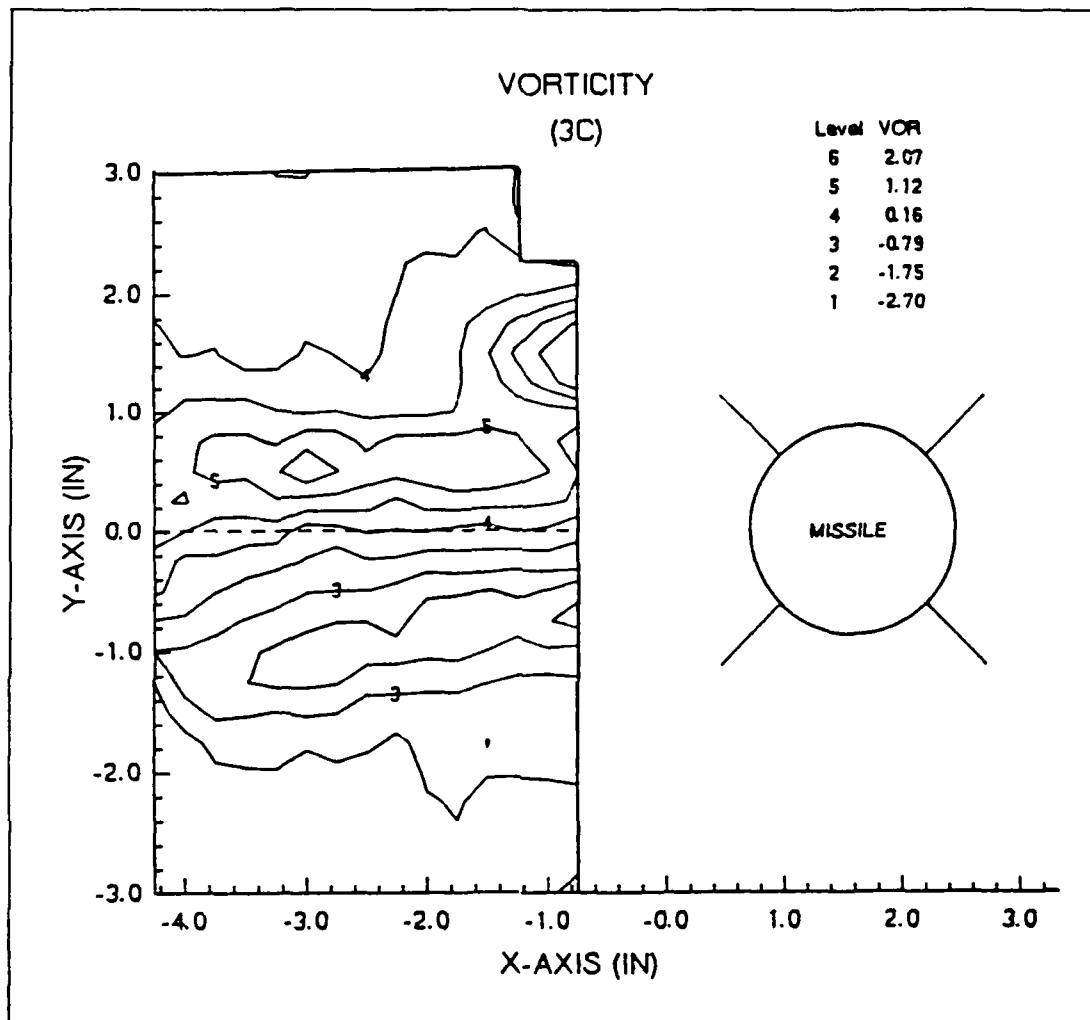


Figure 21. Vorticity - Configuration 3C

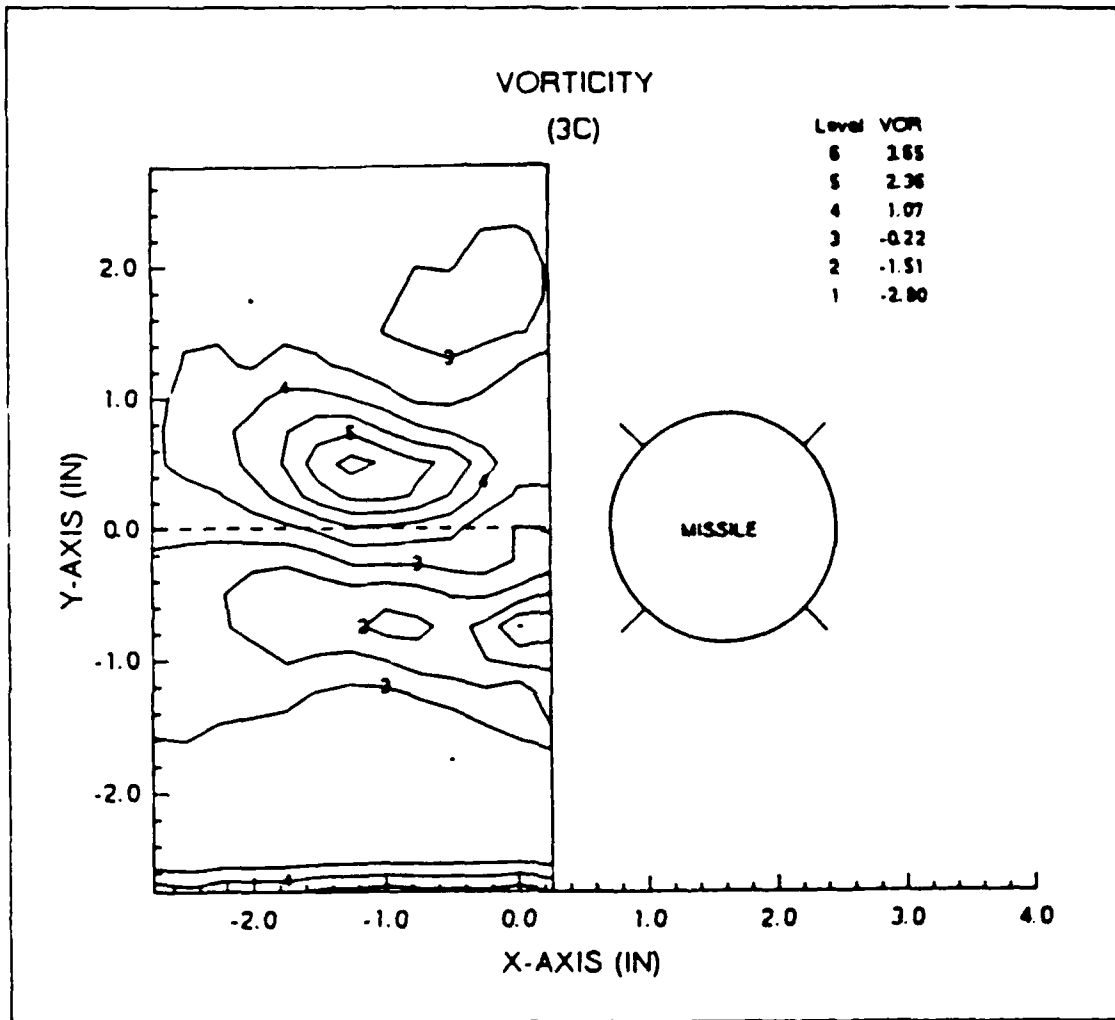


Figure 22. Vorticity (at 6d) - Configuration 3C

F. COMPARISON BETWEEN NO TURBULENCE AND TURBULENCE

For each roll angle, the addition of turbulence on the scale of the vortices did not affect the general shapes of the plots. The effect on the velocities was to decrease the magnitudes but the directions were the same. Total pressure was affected differently for each roll angle. The losses increased for the "+" configuration. The losses decreased for the "x" configuration. The addition of turbulence increased the gradients on the pressure plots. Vorticity strength was less and gradients were reduced. Vorticity plots from Viniotis showed changes that also depended on roll angle. With turbulence, the "+" configuration vorticity had more strength and larger gradients for the centers away from the missile. The closer centers had lower gradients. With turbulence, the "x" configuration vorticity had less strength and lower gradients.

G. COMPARISON BETWEEN ROLL ANGLES

Changing the roll angle from the "+" to the "x" configuration caused significant changes in each of the plots. The velocity plots showed the formation of two vortices below centerline. The total pressure plots showed the two, almost symmetric centers change to one major center located above centerline. The other center is expected to be outside the survey grid. The vorticity plots continued to show four

centers but they move closer to the centerline and closer to the missile. The vorticity plots from Viniotis change depending on the turbulence. Changing from the "+" to the "x" configuration with no turbulence, the centers away from the missile increase in strength and the closer ones have less of a gradient. Changing from the "+" to the "x" configuration with turbulence, the centers are more diffuse.

IV. CONCLUSIONS AND RECOMMENDATIONS

In general, the effect of turbulence in the flowfield on the scale of the vortices was to change the magnitudes of the variables without changing the general shapes of the plots. Velocity and vorticity decreased and vorticity was more diffused. The addition of turbulence affected total pressure changes differently for each roll angle. The locations of the cores of the vortices and the centers of the pressure and vorticity plots shifted little with added turbulence.

Changing the roll angle caused significant changes in the general shapes of the plots, indicating changes in vortex location and size. Two vortices were noted in "+" configuration while the "x" configuration had three vortices. The additional vortices formed on the wings in the "x" configuration appear to reinforce the nose vortex above centerline and force the nose vortex below centerline farther away from the missile. In general, the magnitudes of the variables were lower in the "x" configuration than the "+" configuration. Greater changes in magnitudes were noted with differing turbulence, not with roll angle.

For all four of the configurations, the locations of the vortices indicated by the velocity vector plots did not coincide with the centers of the pressure or vorticity plots.

The differences between the velocity vector plots and the vorticity plots is not suprising, because vorticity is a measure of the velocity gradients. These may not be largest in the core of the vortex.

Rabang noted that the side force magnitudes increased with turbulence on the scale of the vortices in the "+" configuration. The plots indicated that the turbulence increases the losses in total pressure and increases the gradients. The vorticity plot shows a shift in the contour pattern below centerline. For the "x" configuration, Rabang noted that the side force magnitude decreased with the addition of turbulence. The total pressure plot shows that the losses decrease. The centers in the vorticity plot become more elongated.

Recommendations for future reasearch are:

- (1) Conduct flow visualization studies to verify the results of the pressure probe survey.

- (2) Conduct pressure measurements in the area closer to the missile, outside the present survey grid, to determine the characteristics of vortices that may not have been located or observed.

- (3) Conduct pressure measurements on the body without wings/strakes at the 11d position to relate to previous investigations.

APPENDIX A

This program, named CONVERT, inputs the voltage measurements taken from the five ports in the pressure probe, and using ambient conditions and calibration data supplied by the probe manufacturer, computes total velocity, velocity components in the grid plane, total pressure coefficient, and static pressure coefficient.

```
*****
*****
* THIS PROGRAM CONVERTS THE VOLTAGE OF TRANSDUCER INTO
* PHYSICAL *
* PRESSURE, VELOCITY, YAW ANGLE AND PITCH ANGLE. THOSE DATA ARE
*
* USED FOR PLOT PROGRAM LATER.
*
*****
*****
CHARACTER*12 FNAME
CHARACTER*12 NAME
CHARACTER*12 FONAME
CHARACTER*2 A(50)
CHARACTER*80 ST
REAL K, INTR
INTEGER COLS, RWS, DTPTS
DATA A/'01','02','03','04','05','06','07','08','09',
*      '10','11','12','13','14','15','16','17','18',
*      '19','20','21','22','23','24','25','26','27',
*      '28','29','30','31','32','33','34','35','36',
*      '37','38','39','40','41','42','43','44','45',
*      '46','47','48','49','50'/
WRITE (*,'(A\)' ) ' # OF COLS (AWAY FROM MSL) = '
READ (*,'(I5)' ) COLS
WRITE (*,'(A\)' ) ' # OF DATA PTS IN A COL (UP/DOWN) =
,
READ (*,'(I5)' ) RWS
WRITE (*,'(A\)' ) ' DATA FILE NAME? (IE R001A2XX.DAT)
,
READ (*,'(A12)' ) NAME
WRITE (*,'(A\)' ) ' PI (F4.2) = '
READ (*,'(F4.2)' ) PI
```

```

WRITE (*, '(A\)' ) ' PF (F4.2) = '
READ (*, '(F4.2)' ) PF
WRITE (*, '(A\)' ) ' TI (F3.1) = '
READ (*, '(F3.1)' ) TI
WRITE (*, '(A\)' ) ' TF (F3.1) = '
READ (*, '(F3.1)' ) TF
WRITE (*, '(A\)' ) ' K (F6.4) = '
READ (*, '(F6.4)' ) K
WRITE (*, '(A\)' ) ' SLOPE FOR DELTAP (F9.6) = '
READ (*, '(F9.6)' ) SLOPE
WRITE (*, '(A\)' ) ' INTERCEPT FOR DELTAP (F9.6) = '
READ (*, '(F9.6)' ) INTR
WRITE (*, '(A\)' ) ' QM1 FACTOR (F4.2) = '
READ (*, '(F4.2)' ) QM1FAC
WRITE (*, '(A\)' ) ' X OFFSET = '
READ (*, '(F5.2)' ) XOFF
WRITE (*, '(A\)' ) ' Y OFFSET = '
READ (*, '(F5.2)' ) YOFF
WRITE (*, '(A\)' ) ' OUTPUT FILE NAME = '
READ (*, '(A12)' ) FONAME
*   CONVERT THE PRESSURE UNIT FROM inHg TO psf
    PATM=(PI+PF)*35.3631
    R=1716.5
    E=0.0123
    T=(TI+TF)/2.+460
    RO=PATM/(R*T)
    DTPTS=RWS*COLS
*   OPEN A NEW FILE TO STORE THE REDUCED DATA
    OPEN(2, FILE=FONAME, STATUS='NEW')
    WRITE(2, 222) DTPTS
222   FORMAT (I5)
*   OPEN A SEQUENTIAL OF DATA FILE
    DO 20 I=1, COLS
        NAME(7:8)=A(I)
        FNAME=NAME
        OPEN(1, FILE=FNAME)
        READ(1, 100, END=20) ST
100   FORMAT(A65)
15    READ(1, 1000, END=30) NO, X, Y, V1, V2, V3, V4, V5, BETA
1000  FORMAT(I2, F7.2, F6.2, 5F9.3, F8.2)
*   CONVERT THE VOLTAGE TO PRESSURE IN LBF/FT**2
    P1=DELTAP(V1, SLOPE, INTR)*2.0475+PATM
    P2=DELTAP(V2, SLOPE, INTR)*2.0475+PATM
    P3=DELTAP(V3, SLOPE, INTR)*2.0475+PATM
    P4=DELTAP(V4, SLOPE, INTR)*2.0475+PATM
    P5=DELTAP(V5, SLOPE, INTR)*2.0475+PATM
*   CALCULATE THE PITCH ANGLE IN DEGREES
    P=(P4-P5)/(P1-P2)
*   TEST FOR LIMITS IN THE CALIBRATION CURVE
    IF (P.GT.0.80) P=0.80
    IF (P.LT.-0.80) P=-0.80

```

```

      ALPHA=FPITCH(P)
*   CALCULATE THE VELOCITY IN FT/SEC
      YSLOP=FYSLOP(ALPHA)
      VELM=SQRT((2*YSLOP*(P1-P2))/(RO*K))
      VEL=VELM*(1+E)
*   CALCULATE THE LOCAL DYNAMIC PRESSURE
      QM1=QM1FAC*2.0475/K
      QM=RO*VEL**2/2.
      Q1=QM1*(1+2*E)
      Q=QM*(1+2*E)
*   CALCULATE THE YAW ANGLE IN DEGREES
*   YAW (5.0) AND ALPHA(-17.942) CORRECTIONS ARE ADDED
      YAW=FYAW(BETA+5.0)
*   CALCULATE THE VELOCITY COMPONENTS
      BETAR=YAW*.017453
      ALPHAR=(ALPHA-17.942)*.017453
      VELY=VEL*SIN(ALPHAR)
      VELX=VEL*COS(ALPHAR)*SIN(BETAR)
*   CALCULATE THE TOTAL PRESSURE IN LBF/IN**2
      PTC=FPT(ALPHA)
      PT1=P1-Q*PTC
      PT=PT1/144.
      CPT=(PT1-PATM-Q1)/Q1
*   CALCULATE THE STATIC PRESSURE IN LBF/IN**2
      PS1=PT1-Q
      PS=PS1/144
      CPS=(PS1-PATM)/Q1
*   WRITE VALUES TO OUTPUT FILE
      WRITE(2,2000)-X+XOFF,Y+YOFF,VEL,VELX,VELY,YAW,
C      ALPHA-17.942,PT,CPT,PS,CPS
2000      FORMAT(11F10.3)
      GO TO 15
30      CLOSE(1)
20      CONTINUE
      CLOSE(2)
      STOP
      END
*****
*   THIS FUNCTION CONVERTS THE VOLTAGE TO PHYSICAL PRESSURE
      FUNCTION DELTAP(X,SLOPE,INTR)
      REAL INTR
      DELTAP=X*SLOPE+INTR
      END
*****
*   THIS FUNCTION CALCULATES THE PITCH ANGLE
      FUNCTION FPITCH(X)
      FPITCH=3.759+53.7568*X-1.3085*X**2-1.6583*X**3
      *      -0.8061*X**4+16.5115*X**5
      END
*****
*   THIS FUNCTION CALCULATES THE VELOCITY PRESSURE COEFFICIENT

```

```

FUNCTION FYSLOP(X)
IF(X.LT.-10) THEN
  FYSLOP=0.981-0.0102*X-3.000E-4*X**2-2.500E-6*X**3
ELSE IF((X.GE.-10).AND.(X.LE.10)) THEN
  FYSLOP=0.98-0.006*X+2.000E-4*X**2
ELSE
  FYSLOP=0.9801-0.0035*X-1.143E-4*X**2+5.833E-6*X**3
END IF
END
*****
* THIS FUNCTION CALCULATES THE YAW ANGLE
FUNCTION FYAW(X)
IF((X.GE.0).AND.(X.LE.180)) THEN
  FYAW=-X
ELSE
  FYAW=360-X
END IF
END
*****
* THIS FUNCTION CALCULATES THE TOTAL PRESSURE COEFFICIENT
FUNCTION FPT(X)
IF(X.LE.-30) THEN
  FPT=-0.01
ELSE IF((X.GT.-30).AND.(X.LT.-20)) THEN
  FPT=0.02+1.00E-3*X
ELSE IF((X.GE.-20).AND.(X.LE.30)) THEN
  FPT=0
ELSE
  FPT=0.03-1.00E-3*X
END IF
END

```

APPENDIX B

This program, named VORTIC, inputs the velocity components computed in CONVERT and uses a numerical differencing method to obtain the partial derivatives of the velocity components in both the X and Y directions. Vorticity at each point is computed by subtracting the partial derivatives.

```

      CHARACTER*12 FNAME,OFNAME
      REAL VEL,VX(15,25),VY(15,25),VOR(15,25),VORX(15,25)
      REAL VELX,VELY,X,Y,DH,VORY(15,25),XC(15,25),YC(15,25)
      WRITE(*,'(A\)' ) ' DATA FILE NAME ? '
      READ (*,'(A12)' ) FNAME
      WRITE (*,'(A\)' ) ' OUTPUT FILE NAME ? '
      READ (*,'(A12)' ) OFNAME
      OPEN (3,FILE=OFNAME,STATUS='NEW')
      OPEN (2,FILE=FNAME)
10    READ (2,100,END=20) X,Y,VEL,VELX,VELY
100  FORMAT (5F10.3)
C    COMPUTE INDICES FOR ARRAYS
      J=INT((Y/.25)+13.0)
      I=INT((-X/.25)-2.0)
C    COMPUTE NON-DIMEN. VELOCITIES
      VX(I,J)=VELX/VEL
      VY(I,J)=VELY/VEL
      XC(I,J)=X
      YC(I,J)=Y
      GO TO 10
C    COMPUTE NON-DIMEN. STEP SIZE
C    DELTA H=2*GRID STEP DISTANCE/MISSILE DIAMETER
20    DH=(2.0*.25)/1.75
C    COMPUTE VALUES FOR THE Y VORTICITY IN X DIR. ARRAY
      DO 30 J=1,25
      DO 40 I=1,15
C    IF STATEMENTS DEFINE BOUNDARIES
C    FIRST 2 COLUMNS ONLY HAVE 22 POINTS
C    FILE 0A HAS ONLY 21 POINTS
      IF(FNAME.EQ.'0A.DAT'.AND.I.LT.3.AND.J.EQ.1)THEN
        GO TO 40
      ELSE IF(I.LT.3.AND.J.GT.22) THEN
        GO TO 40
      ELSE IF(I.EQ.1) THEN
        VORY(I,J)=(-3.*VY(I,J)+4.*VY(I+1,J)-VY(I+2,J))/DH

```



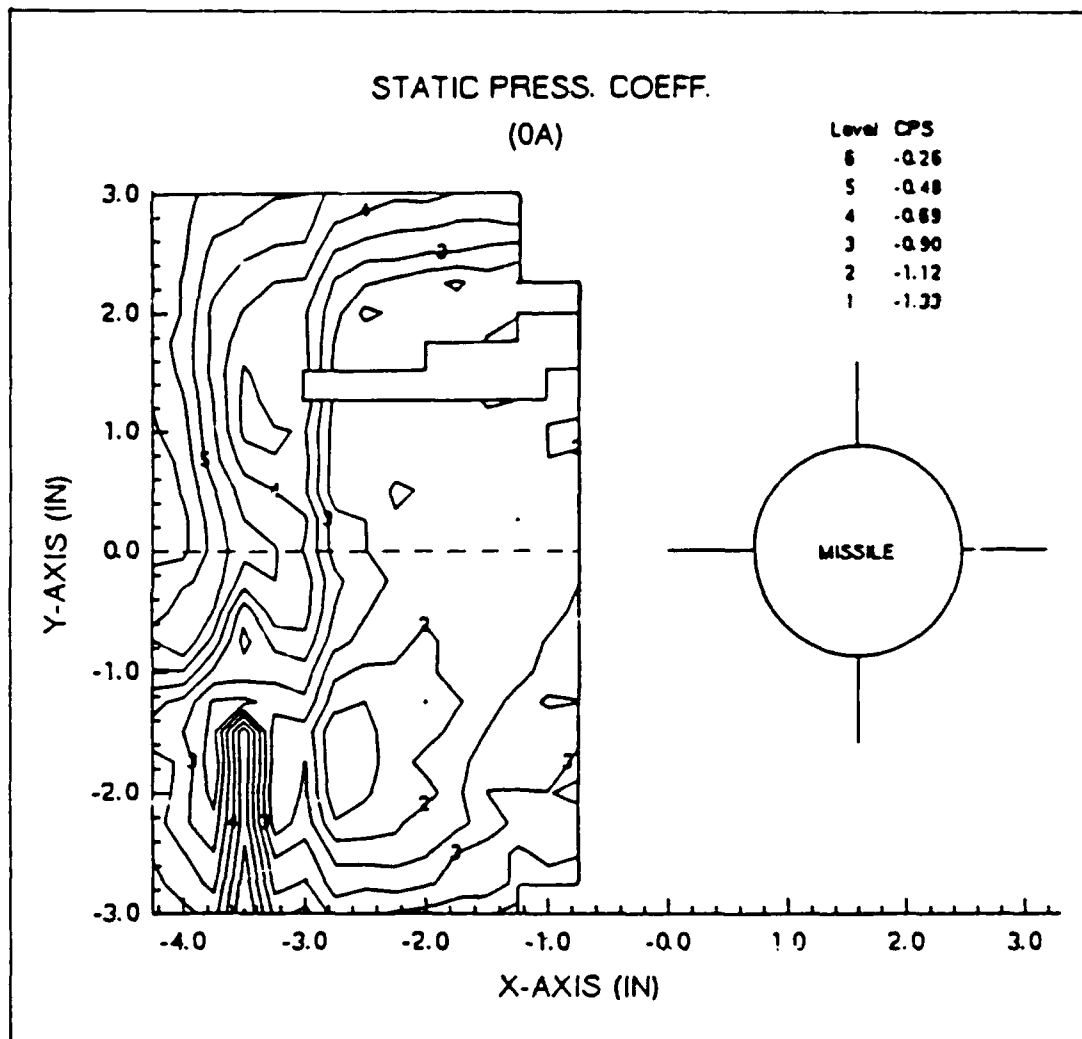
```

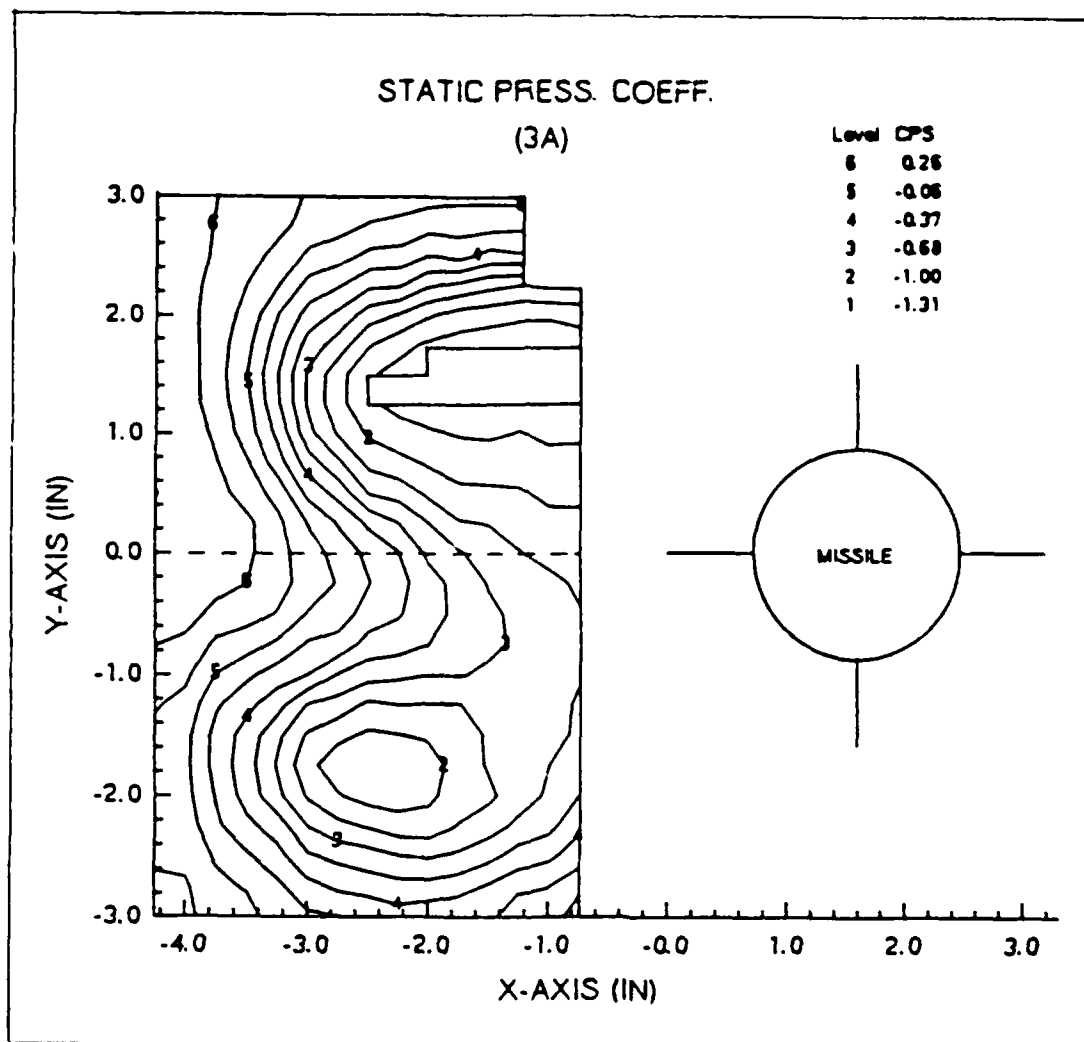
        ELSE IF(I.EQ.15) THEN
            VORY(I,J)=(3.*VY(I,J)-4.*VY(I-1,J)+VY(I-2,J))/DH
        ELSE
            VORY(I,J)=(VY(I+1,J)-VY(I-1,J))/DH
        ENDIF
40    CONTINUE
30    CONTINUE
C    COMPUTE VALUES FOR THE X VORTICITY IN Y DIR. ARRAY
    DO 35 J=1,25
        DO 45 I=1,15
C    IF STATEMENTS DEFINE BOUNDARIES
            IF(FNAME.EQ.'0A.DAT'.AND.I.LT.3.AND.J.EQ.1) THEN
                GO TO 45
            ELSE IF(J.EQ.1) THEN
                VORX(I,J)=(-3.*VX(I,J)+4.*VX(I,J+1)-VX(I,J+2))/DH
            ELSE IF (J.EQ.22.AND.I.LT.3.OR.J.EQ.25.AND.I.GE.3)
THEN
                VORX(I,J)=(3.*VX(I,J)-4.*VX(I,J-1)+VX(I,J-2))/DH
            ELSE IF (J.GT.22.AND.I.LT.3) THEN
                GO TO 45
            ELSE
                VORX(I,J)=(VX(I,J+1)-VX(I,J-1))/DH
            ENDIF
45    CONTINUE
35    CONTINUE
C    COMPUTE THE VORTICITY FOR EACH POINT
    DO 50 I=1,15
        DO 55 J=1,25
            VOR(I,J)=VORY(I,J)-VORX(I,J)
            WRITE (3,200)XC(I,J), YC(I,J), VOR(I,J)
200    FORMAT (3F10.3)
55    CONTINUE
50    CONTINUE
        CLOSE (2)
        CLOSE (3)
        STOP
        END

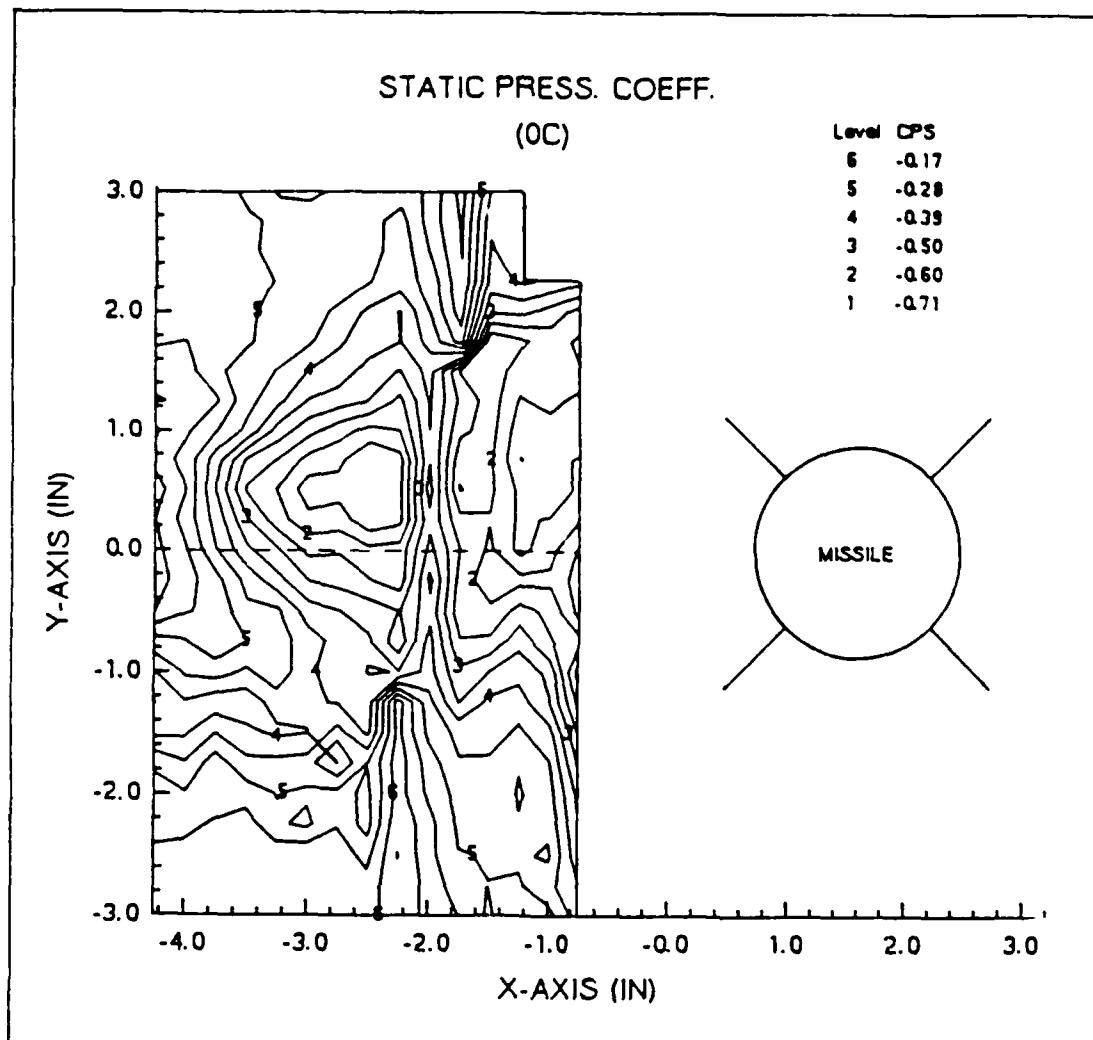
```

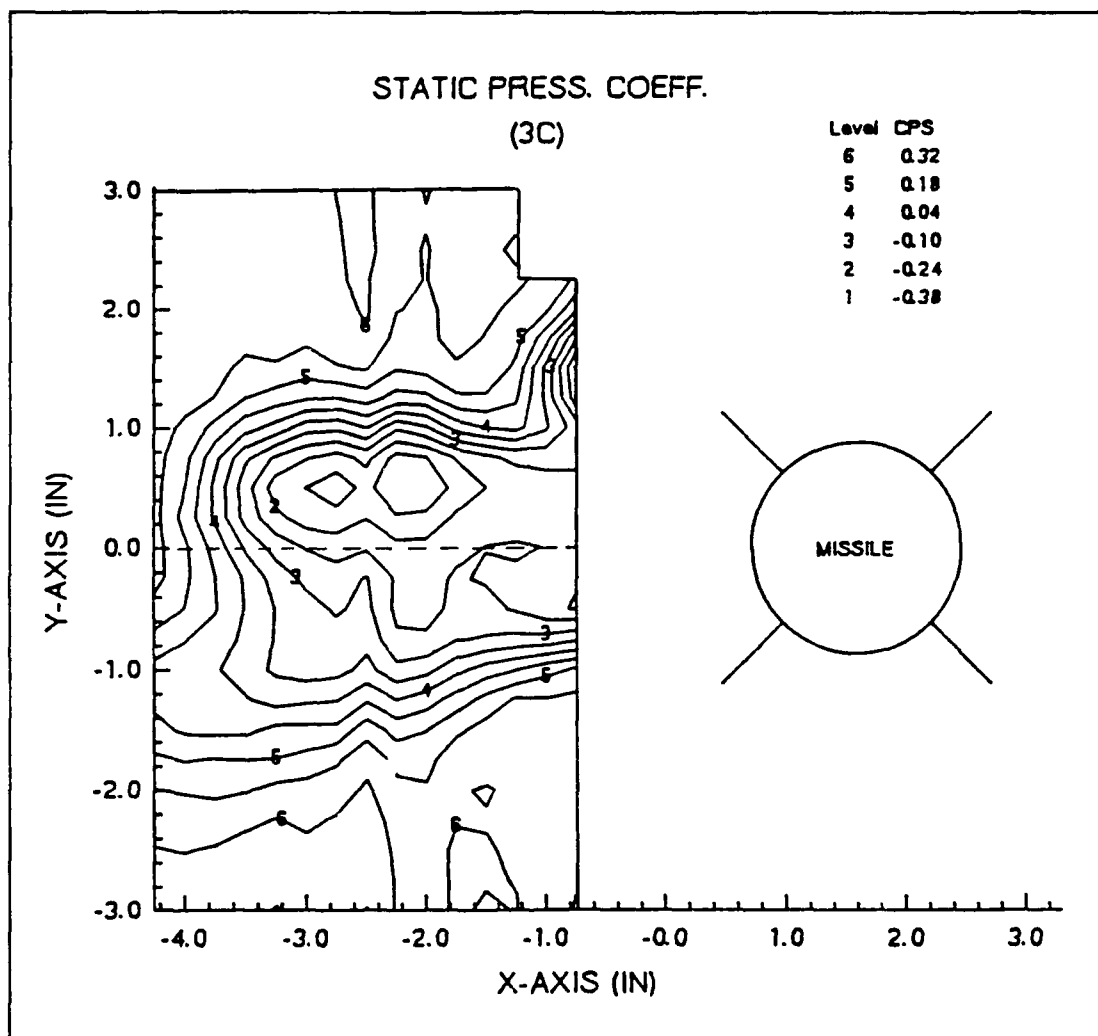
APPENDIX C

The order for the static pressure coefficient contour plots is configuration 0A, 3A, 0C, and 3C.









LIST OF REFERENCES

1. Dahlem, Valentine, and others, *High Angle of Attack Missile Aerodynamics at Mach Numbers 0.3 to 1.5*, AFWAL-TR-80-3070, November 1980.
2. Sheffield, J. Steven, and Deffenbaugh, F.D., *A Three Dimensional Vortex Wake Model for Missiles at High Angles of Attack*, NASA Contractor Report 3208, January 1980.
3. Sheppard, N.M. and Shenton, P.H., *The Asymmetric Shedding of Vortices from an Ogive-Nose Slender Cylinder at Incidence to a Uniform Flow*, Paper, University of Bristol, Bristol, U.K., June 1976.
4. Dunne, Anthony L., and others, *VLA Missile Development And High Angle of Attack Behavior*, NEAR Conference on Missile Aerodynamics Proceedings, Monterey, CA, November, 1988.
5. Ericsson, Lars E. and Redding, J. Peter, *Asymmetric Vortex Shedding from Bodies of Revolution*, Tactical Missile Aerodynamics, American Institute of Aerodynamics and Astronautics, Inc., 1986.
6. Wardlaw, Andrew B., Jr., and Yanta, William J., *Multistable Vortex Patterns on Slender, Circular Bodies at High Incidence*, AIAA Journal, Volume 20, Number 4, pp. 509-515, April 1982.
7. Lung, M.H., *Flowfield Measurements in the Vortex Wake of a Missile at High Angle of Attack in Turbulence*, Master's Thesis, Naval Postgraduate School, Monterey, CA, December 1988.
8. Viniotis, J.J., *Flowfield Effects of Launch on a Vertically-Launched Missile*, Master's Thesis, Naval Postgraduate School, Monterey, CA, June 1989.
9. Deane, J.R., "Missile Body Vortices and Their Interaction with Lifting Surfaces", AGARD/VKI, Lecture Series, no. 121, *High Angle of Attack Aerodynamics*, March 1982.
10. Rabang, M.P., *Turbulence Effects on the High Angle of Attack Aerodynamics of a Vertically-launched Missile*, Master's Thesis, Naval Postgraduate School, Monterey, CA, June 1988.

11. Roane, D.P., *The Effect of a Turbulent Airstream on a Vertically-launched Missile at High Angles of Attack*, Master's Thesis, Naval Postgraduate School, Monterey, CA, December 1987.
12. Tieleman, H.W., *A Survey of the Turbulence in the Marine Surface Layer for the Operation of Low-Reynolds Number Aircraft*, Virginia Polytechnic Institute Report, VPI-E-85-10, Blacksburg, VA, March 1985.
13. Castro, I.P., *Effects of Free Stream Turbulence on Low Reynolds Number Boundary Layers*, Journal of Fluids Engineering, Volume 106, pp. 298-306, September 1984.
14. Meier, H.U. and Kreplin, H.P., *Influence of Freestream Turbulence on Boundary Layer Development*, AIAA Journal, Volume 18, Number 1, pp. 11-15, January 1980.
15. *Laboratory Manual for Slow-Speed Wind Tunnel Testing*, Department of Aeronautics, Naval Postgraduate School, Monterey, CA, 1983.
16. Velmex, Inc., *User's Guide to 8300 Series Stepping Motor Controller/Drivers*, East Bloomfield, NY, January 1988.
17. Hewlett-Packard, Inc., *PC Instruments System Owner's Guide Using HP 610618 System Interface*, February 1986.
18. United Sensors, Inc., *5-Hole Probes Calibration Manual*, Watertown, MA, June 1988.

INITIAL DISTRIBUTION LIST

	No. Copies
1. Library, Code 0142 Naval Postgraduate School Monterey, CA 93943-5002	2
2. Chairman Department of Aeronautics and Astronautics Code 67 Naval Postgraduate School Monterey, CA 93943-5000	1
3. Commander Naval Air Systems Command Washington, DC 20360	1
4. Commander Naval Surface Warfare Center Code G20, ATTN: Dr. Jesse East Dahlgren, VA 22448	2
5. Commander Naval Sea Systems Command Washington, DC 20362-5001	1
6. Commander U.S. Army Missile Command Redstone Arsenal, AL 35898	1
7. Commander U.S. Army Material Command ATTN: AMCPM/FA51 Proponent Officer 5001 Eisenhower Avenue Alexandria, VA 22333-0001	1
8. Commander Naval Weapons Center China Lake, CA 93555	1
9. Commander Pacific Missile Test Center Point Mugu, CA 93042	1

- | | |
|--|---|
| 10. Defense Technical Information Center
Cameron Station
Alexandria, VA 22304-6145 | 2 |
| 11. Federal Aviation Administration
ANS-1, Rm 838
ATTN: David Johnson
800 Independence Avenue
Washington, DC 20591 | 1 |
| 12. Prof. R.M. Howard
Department of Aeronautics and Astronautics
Code 67Ho
Naval Postgraduate School
Monterey, CA 93943-5000 | 6 |